EMERGENT TEMPORAL ABSTRACTIONS IN AUTOREGRESSIVE MODELS ENABLE HIERARCHICAL REINFORCEMENT LEARNING

Seijin Kobayashi[1,*], **Yanick Schimpf**[1,*], **Maximilian Schlegel**[1,*],

Angelika Steger[1], **Maciej Wolczyk**[1], **Johannes von Oswald**[1], **Nino Scherrer**[1], **Kaitlin Maile**[1], **Guillaume Lajoie**[1], **Blake A. Richards**[1], **Rif A. Saurous**[1], **James Manyika**[2], **Blaise Agüera y Arcas**[1], **Alexander Meulemans**[1,*] **and João Sacramento**[1,*]

[1] **Google, Paradigms of Intelligence Team,** [2] **Google,** [*] **Core contributor.**

ABSTRACT

Large-scale autoregressive models pretrained on next-token prediction and finetuned with reinforcement learning (RL) have achieved unprecedented success on many problem domains. During RL, these models explore by generating new outputs, one token at a time. However, sampling actions token-by-token can result in highly inefficient learning, particularly when rewards are sparse. Here, we show that it is possible to overcome this problem by acting and exploring within the internal representations of an autoregressive model. Specifically, to discover temporally-abstract actions, we introduce a higher-order, non-causal sequence model whose outputs control the residual stream activations of a base autoregressive model. On grid world and MuJoCo-based tasks with hierarchical structure, we find that the higher-order model learns to compress long activation sequence chunks onto internal controllers. Critically, each controller executes a sequence of behaviorally meaningful actions that unfold over long timescales and are accompanied with a learned termination condition, such that composing multiple controllers over time leads to efficient exploration on novel tasks. We show that direct internal controller reinforcement, a process we term "internal RL", enables learning from sparse rewards in cases where standard RL finetuning fails. Our results demonstrate the benefits of latent action generation and reinforcement in autoregressive models, suggesting internal RL as a promising avenue for realizing hierarchical RL within foundation models.

1 INTRODUCTION

We are witnessing a revolution in artificial intelligence, driven primarily by autoregressive sequence models. These models, most often built with transformers (Vaswani et al., 2017), are trained using self-supervised next-token prediction on datasets of unprecedented scale (Kaplan et al., 2020). After pretraining, finetuning autoregressive models with reinforcement learning (RL) yields agents with competence in a wide range of domains and tasks, from mathematical problem solving, to being helpful assistants in scientific and creative human endeavors. Currently, there is great interest in leveraging RL as a means to discover new intelligent behaviors, beyond those present in the original training data (Guo et al., 2025).

RL efficiency can be greatly increased by starting from an autoregressive sequence model pretrained on a wide range of behaviors, such as a large language model (LLM). From an RL standpoint, self-supervised pretraining can be seen as imitation learning under partial observability, where not only is noise introduced and intermediate steps occluded, but also latent variables, such as task descriptors, agent rewards and goals, and their mental states, are unknown. This setup imbues the resulting models with latent variable inference capabilities (Xie et al., 2022; Oswald et al., 2023) (commonly referred to as in-context learning (Brown et al., 2020)) that allow adapting to new tasks and environments quickly. Moreover, pretrained autoregressive models provide rich action priors for sampling diverse, meaningful sequences can be sampled, enabling efficient early exploration.

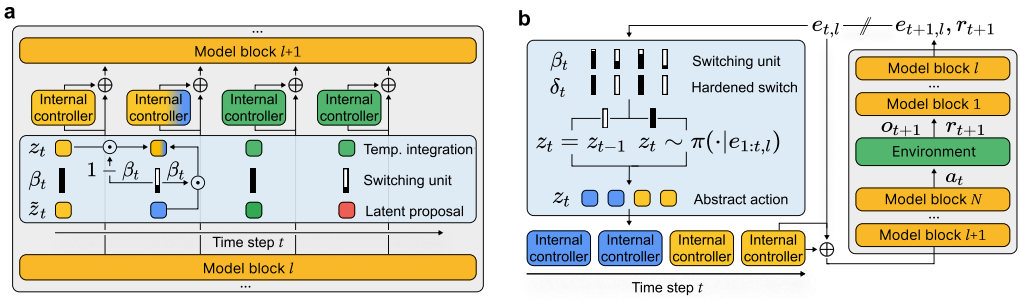

Figure 1: **Research overview.** (**a**) We let a metacontroller steer the residual stream activations of a pretrained autoregressive model. Through self-supervised next-action prediction, the metacontroller discovers how to generate sequences of simple (linear) internal controllers that change sparsely in time, following a dynamic switching unit $\beta_t \in [0, 1]$. In hierarchically-structured tasks, each internal controller corresponds to a temporally-abstract action that leads the base autoregressive model to achieve a meaningful elementary goal. (**b**) We perform RL internally – in the abstract space discovered by the metacontroller – by subsuming the autoregressive model into the environment and acting in the residual stream on a contracted timescale.

Efficient, long-horizon exploration is key for RL to succeed, in particular when rewards are sparse. This leads us to an important problem that autoregressive models face: because these models produce sequences one token at a time, RL exploration is driven entirely by token-level variations. However, solely relying on token-by-token variability to explore can be insufficient to make progress on hard, sparse-reward problems which require generating multiple tokens correctly before obtaining a reward. This observation, which is at the center of the present study, has motivated a long line of research on hierarchical RL. Hierarchical RL attempts to exploit the fact that real-world problems are typically amenable to a hierarchical approach, wherein a final solution is expressed in terms of temporally-abstract actions — i.e., reusable subroutines that run for extended time periods (sometimes called "options") (Sutton et al., 1999). Evidence suggests that humans approach problem solving using such temporal abstractions (Botvinick et al., 2009), which implies that this may be a very efficient way to learn. Importantly, if temporally-abstract subroutines exist, exploration can occur at higher levels of temporal abstraction, drastically reducing the search space relative to token-by-token exploration. However, discovering appropriate subroutines via deep RL remains a longstanding challenge. While policy gradient methods have been derived (e.g., the option-critic (Bacon et al., 2017)), these approaches have theoretical issues and tend to fail in practice, often converging to degenerate options (Pateria et al., 2021).

In this paper, we pursue an alternative approach for temporally-abstract action discovery that builds directly upon autoregressive modeling. Based on their in-context latent variable inference capabilities, we hypothesize that autoregressive action models implicitly learn temporally-abstract actions represented in their internal activations, despite being trained to predict only one token at a time. This hypothesis leads us to introduce an internal neural network controller in charge of steering the internal activations of a base model. Critically, the controller learns through an unsupervised variational inference algorithm (Peterson, 1987; Hinton & van Camp, 1993; Kingma & Welling, 2014; Rezende et al., 2014), which does not require per-time-step abstract action labels, in contrast to standard model steering techniques (Zou et al., 2023; Turner et al., 2023).

We evaluate our approach on a family of RL tasks that are constructed in a hierarchical, compositional manner. We consider both a classic discrete grid world environment (Kipf et al., 2019; Jiang et al., 2022), and a more challenging hierarchical continuous control environment implemented on the MuJoCo physics simulator (Todorov et al., 2012). The latter requires an agent to master both low-level continuous motor control as well as planning at a higher level of temporal abstraction to exploit the underlying discrete, compositional task structure. We find that the internal controller discovers how to generate higher-order sequences of temporally-abstract actions that switch sparsely in time. These abstract actions enable efficient exploration by drastically reducing the search space size in novel tasks and simplify credit assignment by reducing the effective time horizon of the policy. The final product is *internal RL* – a novel hierarchical RL method that acts within an autoregressive model, and which directly reinforces internal activations to solve sparse reward tasks that token-

level approaches cannot solve. Our results demonstrate the benefits of latent action generation for RL applied to pretrained autoregressive models.

2 ENVIRONMENT DESIGN AND BASE MODEL PRETRAINING

Before diving into the description of our internal RL model acting in a pretrained autoregressive model, we first describe the pretraining of such a base model alongside the environment setup and (pre)training data considered in this work. We pretrain our models from scratch on a behavioral dataset D comprising observation-action sequences produced by different expert agents that solve tasks via stochastic policies of varying degrees of optimality. The autoregressive model can thus be thought of as a sequence model of likely observation-action trajectories. Each element of D is a sequence $(o_1, a_1, \ldots, a_T, o_{T+1})$ comprised of the initial sensory observations o_1, actions a_t taken by an agent and resulting sensory observation o_{t+1} at time steps $t \in \{1, \ldots, T\}$. Like behavioral datasets collected at scale (e.g., those used to train LLMs), D does not contain rewards, nor any explicit agent goal and task descriptors. The analyses presented in this section seek to determine if, and how, autoregressive models infer abstract patterns in long-horizon, goal-directed action sequences.

We collect behavior from two classes of environments where agents perform navigation tasks. Importantly, the tasks are hierarchically-structured (cf. Fig. 2): though basic movement skills are a prerequisite, any given task can be solved with a combination of sub-routines composed of common sequences of basic movements. More concretely, we study both a discrete grid world environment that was previously introduced as a testbed for hierarchical RL (Kipf et al., 2019; Jiang et al., 2022), as well as a continuous-observation, continuous-action adaptation implemented by us in the MuJoCo physics simulator (Todorov et al., 2012), where a quadrupedal robot (the 'ant' (Schulman et al., 2015; Fu et al., 2020)) must be controlled at joint-level. In both environments, an agent needs to follow a course that arrives at certain colored locations in a specific order. In other words, the agents need to navigate between subgoals while also ignoring distractors (non-goal colored locations), all while avoiding collisions with randomly placed walls. Any task is described by a sequence of subgoals, which are either a single colored location for the ant, or two consecutive colored locations for the grid world. A given task can be mapped to different spatial configuration of the subgoals, the distractors, and the walls, see Appendix A for more details on the environments. In these environments, abstract actions are equivalent to moving towards a specific subgoal, hence we use the terms "abstract action" and "subgoal" interchangeably in this paper.

Given behavioral data collected for a set of easy tasks, referred to as pretraining tasks set (see Appendix A and C.1 for more details on the tasks and how the behavioral data are collected), we proceed with autoregressive sequence model pretraining, here a standard causal transformer (Vaswani et al., 2017) for discrete grid world data, and an efficient SSM (Hawk (De et al., 2024)) for ant control data. The models are pretrained from scratch by minimizing the cross-entropy

$$L(\theta) = \sum_{(o_{1:T+1}, a_{1:T}) \sim D} \sum_{t=1}^{T} -\ln p_\theta(a_t | o_{1:t}) - \lambda \ln p_\theta(o_{t+1} | o_{1:t}),$$

with p_θ the sequence model, and θ its parameters. For the case of continuous actions, the likelihood $p_\theta(a_t|o_{1:t})$ is modeled as a Gaussian with learned diagonal covariance matrix. For discrete actions, the likelihood is parameterized as a categorical distribution with probabilities provided by the softmax over the output logits. Note that while the main objective here is behavioral (next-action) prediction, the models are also trained on next-observation prediction, the objective of world (dynamics) modeling (Schmidhuber, 1990; Sutton, 1991; Hafner et al., 2025). The weight of this auxiliary loss is determined by a scalar hyperparameter $\lambda \geq 0$; we analyze its role in the Appendix Fig. A4. Additional optimization and architectural details may be found in Appendix C and D.

3 UNSUPERVISED METACONTROLLER DISCOVERS TEMPORALLY-ABSTRACT ACTIONS WITHIN AUTOREGRESSIVE MODELS

Internal activation analyses and causal intervention experiments (c.f. Appendix B.1 and B.2) demonstrate that pretrained autoregressive models naturally learn to represent temporally-abstract actions, and that these representations can be steered using simple linear controllers. Building on these

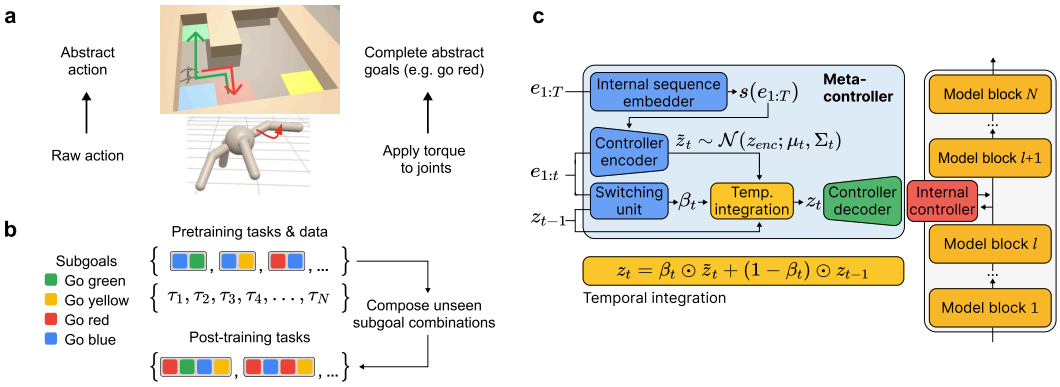

Figure 2: **Environments and Metacontroller architecture.** (**a**) To complete a task, an agent must visit in sequence a number of subgoal locations, each marked with a specific color. A task can be described as an abstract action (subgoal) sequence, or as a sequence of low-level motor commands. (**b**) We pretrain autoregressive action models and metacontrollers on unlabeled behavioral datasets containing observation-action sequences of expert agents performing different tasks. We then test the ability of the models to learn with RL tasks that comprise longer subgoal sequences, combined in new, unseen orders. (**c**) The metacontroller learns in a self-supervised way to generate sequences of internal controllers. Candidate controller codes $\tilde{z}_t$ are sampled from a context-dependent Gaussian, and are integrated at a continuous, time-varying rate β_t, dynamically determined by a switching unit. During self-supervised learning, the metacontroller is non-causal, and has access to the entire sequence of residual stream activations through a sequence embedding $s(e_{1:T})$.

insights, we investigate the more challenging setting where the model must both discover these temporally-abstract actions from an unlabeled behavioral dataset and learn a selection mechanism to achieve larger goals. To do so, we freeze the autoregressive model after training on D and augment it with a metacontroller that learns to generate abstract actions acting on the residual stream of this frozen base model. Inspired by the effectiveness of LoRA finetuning (Hu et al., 2022), we introduce low-rank linear residual stream controllers with parameters $U \in \mathbb{R}^{n_e \times n_e}$ as the action primitives of the metacontroller. Once spawned by the metacontroller, such a low-rank controller U_t modifies the instantaneous residual stream activations in between model blocks at a given depth l following

$$e_{t,l} \leftarrow e_{t,l} + U_t e_{t,l}. \tag{1}$$

Note that by mechanisms detailed later in this section, the metacontroller can chose to maintain such a low-rank controller for multiple subsequent timesteps thereby effectively acting on a temporally abstract timescale (decoupled from the token-space timescale). We continue training on a behavioral dataset D_* with θ fixed. This dataset contains behavioral sequences that are generated in the same way as those in the pretraining dataset D, but with increased optimality D_*. In this second stage of training, the metacontroller learns how to generate the appropriate controllers at the appropriate times. We describe the metacontroller in full in Appendix D.2, and illustrate it in Fig. 2. Briefly, the metacontroller is a generative stochastic recurrent neural network with an encoder-decoder architecture that enables sampling controllers sequentially. Because it outputs the parameters U_t of a controller and not directly a control vector, the metacontroller can be qualified as a recurrent hypernetwork (Ha et al., 2017). The decoder is a feedforward network that produces a controller, U_t, from a controller code, z_t. The encoder is a recurrent network based on the gated recurrent unit (Cho et al., 2014) that specifies the mean μ_t and variance Σ_t of a Gaussian distribution over a random controller code $\tilde{z}_t \sim \mathcal{N}(z_{\text{enc}}; \mu_t, \Sigma_t)$. Importantly, the encoder is non-causal, because it receives an embedding, $s(e_{1:T})$, of the whole sequence of latent activities. We justify such future-conditioning using a formal latent variable modeling argument in Appendix E.1.

Additionally, the metacontroller includes a recurrent switching unit, that operates between the encoder and decoder. This unit determines a time-varying continuous switching gate $\beta_t \in [0, 1]$, which controls the interpolation between previous controller code z_{t-1} and a new sampled code $\tilde{z}_t$:

$$z_t = \beta_t \odot \tilde{z}_t + (1 - \beta_t) \odot z_{t-1}, \tag{2}$$

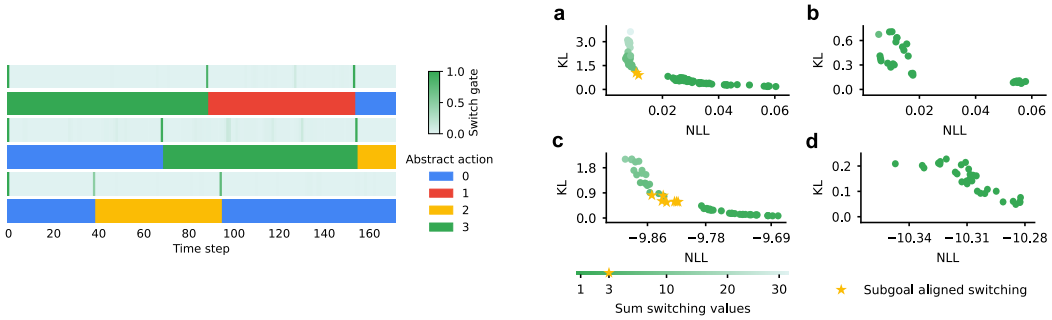

Figure 3: **Discovery of subgoal-aligned switching.** *Left*: Three example trajectories from the ant control environment showing the switch β_t used for temporal integration at each timestep, and the groundtruth abstract action (color-coded). Switching ($\beta_t \approx 1$) coincides with a change in the abstract action being performed. *Right*: We compare the metacontroller steering a frozen base model (left column; **a**, **c**), with a metacontroller that is co-trained with the steered base model (right column; **b**, **d**). The x-axes show the negative log-likelihood (NLL; the distortion) and the y-axes show the KL divergence to the prior (the rate). These rate-distortion curves reveal that subgoal aligned switching (marked with a $\star$) is only discovered with a frozen base model. This holds for grid world (top row; **a**, **b**) and ant environment (bottom row; **c**, **d**).

where $\odot$ denotes elementwise multiplication. Despite its simplicity, this temporal integrator is critical for the metacontroller to learn to generate the appropriate temporally-abstract actions, as we will confirm through ablation experiments at the end of this section.

The metacontroller parameters ϕ are trained through the minimization of a self-supervised learning objective, comprising (low-level) next-action prediction and a prior-matching regularizer,

$$L(\phi) = \sum_{(o_{1:T+1}, a_{1:T}) \sim D_\star} \sum_{t=1}^{T} \Big[-\ln p_{\theta,\phi}(a_t | o_{1:t}, z_{1:t}) + \alpha D_{\mathrm{KL}}\big(\mathcal{N}(\mu_t, \Sigma_t) \,\|\, \mathcal{N}(0, I)\big) \Big], \tag{3}$$

where $D_{\mathrm{KL}}(\cdot \,\|\, \cdot)$ denotes the Kullback-Leibler divergence (Cover & Thomas, 2006). The inclusion of this regularizer (with weight determined by the hyperparameter $\alpha \geq 0$) promotes the generation of meaningful sequences when sampling controller codes z_t from a standard normal distribution, a property that we exploit in the next section to develop a novel hierarchical RL algorithm. From an information-theoretic perspective, α also controls the variational bottleneck by regulating the information flow from the acausal encoder to the controller. As shown in our later analysis, this bottleneck is instrumental in driving the model toward sparse, subgoal-aligned switching patterns that mirror the underlying task structure. Moreover, the choice of an unconditional prior (i.e., abstract action proposals are independent of past ones) promotes the development of compositional representations. In Appendix E.1, we derive eq. (3) formally using a variational information-theoretic approach (Alemi et al., 2018). The derivation is standard, and follows closely previous calculations for stochastic recurrent models (e.g., Linderman et al., 2017; Kim et al., 2019).

Ultimately, the metacontroller both discovers the temporally-abstract actions that underlie the observed agents' behavior, and learns to sequence them appropriately in time by implementing respective termination conditions via the switching gate. In Fig. 3 and A5, we analyze the residual stream controllers discovered by the metacontroller by plotting the switching gate values β_t against groundtruth abstract actions g_t. We find that the metacontroller recovers the groundtruth abstract action switching times. After training, the switch gate learns to behave in a quasi-binary, sparsely-switching fashion, despite not being explicitly regularized to do so. This is a notable finding in light of the critical role that switching regularization methods play in hierarchical RL (Harb et al., 2018), and given the simplicity of the temporal integrator (eq. (2)). The resulting temporal segmentation is essentially perfect, despite the fact that both observations and actions are continuous for the ant environment. Moreover, the metacontroller learns to generate latent controller codes which correspond to meaningful temporally-abstract actions (e.g., "go to color blue"), that generalize to new task configurations and switching times (see Appendix B.4.2 for an analysis).

We next study what happens when the autoregressive base model parameters θ are not kept frozen but co-trained with metacontroller parameters ϕ through variational inference (the minimization of eq. (3), now w.r.t. both θ and ϕ). This baseline is conceptually close to previous hierarchical RL methods that use variational inference to learn abstractions from unlabeled demonstrations (e.g., (Kipf et al., 2019; Jiang et al., 2022)), while using our particular architecture. To compare the abstract action representations developed in a frozen vs. co-trained base model, we conduct a rate-distortion analysis (Alemi et al., 2018), obtained by varying the value of α (which controls the rate-distortion trade-off in eq. (3)) over a wide interval, see C.6 for additional details. We trace rate-distortion curves for our standard metacontroller (which steers a pretrained, frozen autoregressive model) and for the co-trained metacontroller, see Fig. 3. Intriguingly, we find that a horizontal gap appears on the rate-distortion curve between metacontrollers with subgoal-aligned switching (with rate-distortion points marked by a $\star$ symbol in Fig. 3), and those with slightly less rate. This indicates that at that rate level, a small rate increase dramatically improves the distortion. In contrast, for the co-trained metacontroller, although the variational objective is minimized, this structure is lost. For most values of α, the model converges to a degenerate solution characterized by a single switch at the very beginning of the sequence. The fact that subgoal-aligned switching corresponds to this improved distortion with frozen autoregressive models, but not with co-trained models, shows that pretraining builds an internal representation that aligns well with abstract actions. Furthermore, this also has optimization implications: for a given value of α, the variational objective (eq. (3)) is minimized on the point of the rate distortion curve which has a tangent of slope $-1/\alpha$. A gap like the above, with a slope discontinuity, indicates that for a large range of values of α, the variational objective is minimized precisely at the region with subgoal-aligned switching.

Taken together, the results presented in this section provide strong evidence that our model can both learn temporally-abstract actions and how to sequence them appropriately, all in a self-supervised manner. We will see next how this model can be leveraged to speed up exploration in new, harder tasks by many orders of magnitude, enabling sparse-reward RL to succeed.

4 INTERNAL REINFORCEMENT LEARNING

Finally, we consider the question of how to leverage our model to learn harder tasks through hierarchical RL. We study only the challenging sparse-reward setting, where a single positive success reward is provided per trajectory, and only when an entire sequence of subgoals is completed.

We begin this section by establishing that our tasks (described in Fig. 2) are difficult for standard RL approaches to post-training. We first study an adapted version of the GRPO algorithm (Guo et al., 2025), which is a strong baseline in the sparse-reward setting. The details of our GRPO implementation can be found in Appendix C.5.2. For the tasks considered here, training an agent from scratch directly with RL has, for all practical purposes, no chance of succeeding. Thus, to make the comparison fair, we instead apply GRPO to the pretrained autoregressive sequence model, as is now routinely done with LLMs. However, even with a sequence model pretrained on action sequences related to the subgoals, there is only a minuscule chance (on the order of one in a million) of producing successful trajectories by sampling at the output token-level. This causes GRPO training to fail, as the model does not receive enough signal to learn, see Fig. 4. An inspection of the action sequences generated by the autoregressive sequence model reveals that while the model reproduces action sequences seen in the training data, it fails to explore at a higher level of temporal abstraction, which would be required to solve these sparse reward tasks. In other words, training the sequence model with policy gradients does not lead the system to explore novel combinations of subgoals.

Having shown that standard post-training RL fails, we now introduce internal RL. Conceptually, the key step is to treat the autoregressive sequence model as part of the environment; actions then correspond to residual stream interventions, u_t, and observations correspond to residual stream activations, $e_{t,l}$. We note that performing RL at the residual stream level is *a priori* challenging. Consider the problem of learning from scratch a policy $\pi(u_t \mid e_{1:t})$ whose outputs $u_t \in \mathbb{R}^{n_e}$ additively control the residual stream, $e_{t,l} \leftarrow e_{t,l} + u_t$, without relying on error backpropagation to differentiate through the base model that is being controlled. This is a high-dimensional continuous control problem, an exceedingly difficult setting for RL (Lillicrap et al., 2016).

Instead of directly attempting to learn a residual stream control policy, internal RL implements a policy in the controller code space of z, after the metacontroller is trained as described in the

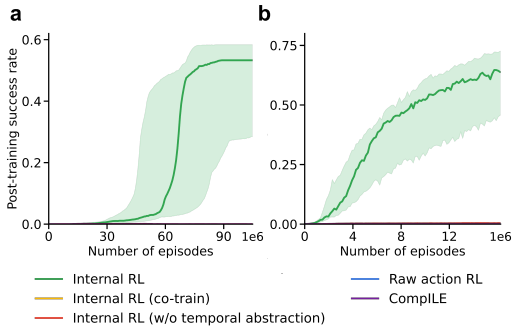

Figure 4: **Internal RL solves sparse-reward compositional tasks where baselines fail.** RL curves for various methods leveraging a pretrained autoregressive model for the (**a**) discrete grid world environment, and (**b**) the ant continuous control environment. All baselines fail to learn within a million episodes while internal RL achieves high success rates. Lines and shaded area resp. report median and the spread between the 25^{th} and 75^{th} quantiles computed over 30 runs.

previous section. This approach assumes that the metacontroller has learned a meaningful switching unit f_{switch}, and a controller code space such that $z_t \sim \mathcal{N}(0, I)$ is a meaningful prior for sampling abstract actions. Intuitively, the metacontroller does not suffer from the drawbacks of directly doing RL in the residual stream for two reasons: (i) the action space dimension is reduced ($n_z < n_e$), (ii) the metacontroller operates on an abstract timescale, dramatically reducing the effective time horizon. The latter is the key property that can enable internal RL to be more efficient and succeed on hierarchical, sparse reward tasks where standard RL methods fail. In more detail, internal RL consists in replacing an unsupervised controller encoder which uses privileged future information $s(e_{1:T})$ by a causal abstract action policy $\pi(z_t \mid e_{1:t})$, and then training it through RL, while keeping the parameters of all other modules fixed. This amounts to subsuming the autoregressive model, and parts of the metacontroller, into the environment (cf. Fig. 1). To generate discrete switching events, we further apply a threshold to binarize the switching rate, i.e., we replace β_t in eq. (2) by $H(\beta_t - \beta_{\text{threshold}})$ with H the Heaviside step function and $\beta_{\text{threshold}} \in \mathbb{R}$ a hyperparameter. This way, until a switch signal ($\beta_t = 1$) is emitted by the metacontroller, the same abstract action is applied, thus allowing π to operate on a temporally-abstract timescale. Pseudocode for the internal RL environment and algorithm is provided in Appendix C.5.1.

Fig. 4 shows that internal RL achieves a high success rate on the post-training tasks. Leveraging the temporal abstractions discovered through self-supervised metacontroller learning is crucial for this success, as shown by the failure of a metacontroller for which the temporal integration is disabled ($\forall_t\ \beta_t = 1$). To give this baseline a fair chance, this ablation is introduced during self-supervised metacontroller learning, not just when performing post-training RL. Intriguingly, the $\beta_t = 1$ ablation also achieves a high initial success rate; this can be seen when plotting success rates in log-scale (cf. Appendix Fig. A7). However, only with temporal-abstraction enabled internal RL both achieves high initial success rates and performs efficient credit assignment, such that RL succeeds. In Appendix E.2 we present a mathematical argument for the efficiency of credit assignment in internal RL, comparing the variance of the policy gradients of internal against RL in raw action space.

Moreover, to evaluate the internal abstractions developed during pretraining, we compare again to the co-trained baseline (optimizing metacontroller and base model to jointly minimize eq. (3)). Consistent with the rate-distortion analysis results (Fig. 3), the success rate of post-training internal RL remains close to zero. The same holds for CompILE (Kipf et al., 2019), a comparable, previously proposed hierarchical RL method that also relies on variational inference to discover temporally-abstract actions from an unlabeled behavioral dataset. These results again confirm the importance of autoregressive pretraining, followed by base model freezing, for enabling hierarchical RL.

5 Discussion

In this work, we asked whether the latent representations of autoregressive sequence models could be leveraged to develop RL techniques that overcome the inefficiency of token-by-token explo-

ration and reinforcement. We studied this question using tasks for which the overall goal is a composition of multiple subgoals. We first showed that an autoregressive sequence model trained on action-observation sequences from experts solving simpler versions of the tasks learn internal representations that carry information about the subgoals. Next, we demonstrated that these latent representations are linearly controllable and, moreover, that the respective low-rank controllers compositionally generalize to complete arbitrary subgoal sequences. We then developed a model that uses a metacontroller to select appropriate temporally-abstract actions without supervision on the groundtruth subgoal labels. Finally, we showed that directly reinforcing the internal activation controllers generated by the metacontroller enables learning in complex, hierarchical sparse-reward tasks where other RL techniques fail. Altogether, our results demonstrate that the latent representations of autoregressive sequence models can be leveraged to enable efficient, hierarchical RL.

A number of prior analyses have probed the internal representations of autoregressive models, looking for temporal abstractions and plans. A recent exciting study provided compelling evidence for planning in LLMs asked to write rhyming poems (Lindsey et al., 2025), and earlier probing work found that hidden LLM states have some predictive power over a short number (four) of future tokens (Pal et al., 2023). Another line of prior work has focused on models trained from scratch in controlled environments, as we do here, notably in games such as Othello (Li et al., 2023; Nanda et al., 2023) or chess (Jenner et al., 2024; Karvonen, 2024). To the best of our knowledge, we are the first to consider continuous environments with a hidden, discrete, hierarchical task structure. Despite being trained by gradient descent and only employing continuous units (both within the base SSM next-token predictor and the metacontroller) the models nonetheless discovered the underlying discrete latent task structure. In particular, the metacontroller developed sparse, quasi-binary switching units. Moreover, our findings complement recent analyses of convolutional LSTM policies trained by end-to-end RL to play the Sokoban game (Bush et al., 2025; Taufeeque et al., 2024). These studies showed that RL led to the development of planning subroutines that unfold over multiple timesteps, like the goal-reaching policies that we found within self-supervised autoregressive models. We complement these studies by focusing on autoregressive transformers and SSMs trained on a next-token prediction objective, the current workhorse of artificial intelligence systems.

Schmidhuber theorized in a seminal paper (Schmidhuber, 2015) that a wake-sleep training loop iterating between training a history compressor through self-supervised learning (SSL), and letting a controller use the internal representations of the former to generate new experiences through RL, would lead to the acquisition of evermore complex capabilities, including the ability to form and exploit temporal abstractions and plans. Here, we provide both a concrete neural architecture following this philosophy, and a set of experimental results backing these claims. Interestingly, we begin to see the benefits of alternating between SSL and RL in large-scale models. For instance, DeepSeek-R1 (Guo et al., 2025) training also involved one iteration of the RL-SSL cycle, albeit with additional human curation involved in the (post-RL) SSL phase, and with RL still done at (raw) output action level.

Our model also displays similarities to LeCun's joint embedding predictive architecture (JEPA; LeCun, 2022). In particular, the metacontroller is similar to the JEPA configurator module, as both are in charge of modulating a general world model and policy in service of a given task/goal. However, JEPA is a proposal for learning abstract observation and action representations without an autoregressive predictive model, whereas next-action prediction is precisely at the center of our approach. In fact, we show that learning a (raw) action predictor is partly what enables discovering how to decompose a task into a sequence of subgoals, one of the open problems in the JEPA proposal.

Finally, our results open a new avenue for model interpretability and control at scale. Similarly to sparse autoencoders (SAEs), a popular method for model interpretability and steering, the metacontrollers introduced in this work can be trained through scalable self-supervised learning and employ an encoder-decoder-type architecture. However, the two models otherwise have significant differences. While SAEs are trained on instantaneous internal activation reconstruction, metacontrollers are predictive and interventive, trained to directly lower output next-token prediction error by intervening on the residual stream. Moreover, they maintain internal state, whereas SAEs are instantaneous. Metacontrollers are thus by design likely better suited if the goal is foundation model control, and they offer the possibility of discovering interpretable interventions that run over an extended period of time. We are excited about the prospect of investigating whether these capabilities translate to larger-scale models such as LLMs.

Acknowledgements. We would like to thank Razvan Pascanu, Jörg Bornschein, Rajai Nasser, Marissa A. Weis, James Evans, Eric Elmoznino, Sangnie Bhardwaj, Charlotte Frenkel, Anoop Sinha, Zoltan Szabadka, Dileep George, Kevin P. Murphy and Doina Precup and her lab members for helpful comments and discussions, as well as Yul Kwon and Alice Guan for overall support.

REFERENCES

Guillaume Alain and Yoshua Bengio. Understanding intermediate layers using linear classifier probes. In *International Conference on Learning Representations*, 2017.

Alexander Alemi, Ben Poole, Ian Fischer, Joshua Dillon, Rif A Saurous, and Kevin Murphy. Fixing a broken ELBO. In *International Conference on Machine Learning*, 2018.

Pierre-Luc Bacon, Jean Harb, and Doina Precup. The option-critic architecture. In *Proceedings of the AAAI Conference on Artificial Intelligence*, 2017.

Maximilian Beck, Korbinian Pöppel, Markus Spanring, Andreas Auer, Oleksandra Prudnikova, Michael Kopp, Günter Klambauer, Johannes Brandstetter, and Sepp Hochreiter. xLSTM: Extended long short-term memory. In *Advances in Neural Information Processing Systems*, 2024.

Matthew M Botvinick, Yael Niv, and Andrew G Barto. Hierarchically organized behavior and its neural foundations: a reinforcement learning perspective. *Cognition*, 2009.

Tom Brown, Benjamin Mann, Nick Ryder, Melanie Subbiah, Jared D Kaplan, Prafulla Dhariwal, Arvind Neelakantan, Pranav Shyam, Girish Sastry, Amanda Askell, Sandhini Agarwal, Ariel Herbert-Voss, Gretchen Krueger, Tom Henighan, Rewon Child, Aditya Ramesh, Daniel Ziegler, Jeffrey Wu, Clemens Winter, Chris Hesse, Mark Chen, Eric Sigler, Mateusz Litwin, Scott Gray, Benjamin Chess, Jack Clark, Christopher Berner, Sam McCandlish, Alec Radford, Ilya Sutskever, and Dario Amodei. Language models are few-shot learners. *Advances in Neural Information Processing Systems*, 2020.

Thomas Bush, Stephen Chung, Usman Anwar, Adrià Garriga-Alonso, and David Krueger. Interpreting emergent planning in model-free reinforcement learning. *arXiv preprint arXiv:2504.01871*, 2025.

Kyunghyun Cho, Bart Van Merriënboer, Dzmitry Bahdanau, and Yoshua Bengio. On the properties of neural machine translation: Encoder-decoder approaches. *arXiv preprint arXiv:1409.1259*, 2014.

Thomas M Cover and Joy A Thomas. *Elements of Information Theory*. Wiley-Interscience, 2006.

Soham De, Samuel L. Smith, Anushan Fernando, Aleksandar Botev, George Cristian-Muraru, Albert Gu, Ruba Haroun, Leonard Berrada, Yutian Chen, Srivatsan Srinivasan, Guillaume Desjardins, Arnaud Doucet, David Budden, Yee Whye Teh, Razvan Pascanu, Nando De Freitas, and Caglar Gulcehre. Griffin: Mixing gated linear recurrences with local attention for efficient language models. *arXiv preprint arXiv:2402.19427*, 2024.

Justin Fu, Aviral Kumar, Ofir Nachum, George Tucker, and Sergey Levine. D4RL: datasets for deep data-driven reinforcement learning. *arXiv preprint arXiv:2004.07219*, 2020.

Atticus Geiger, Hanson Lu, Thomas Icard, and Christopher Potts. Causal abstractions of neural networks. *Advances in Neural Information Processing Systems*, 2021.

Albert Gu and Tri Dao. Mamba: Linear-time sequence modeling with selective state spaces. In *Conference on Language Modeling*, 2024.

Daya Guo, Dejian Yang, Haowei Zhang, Junxiao Song, Ruoyu Zhang, Runxin Xu, Qihao Zhu, Shirong Ma, Peiyi Wang, Xiao Bi, and others. DeepSeek-R1: incentivizing reasoning capability in LLMs via reinforcement learning. *arXiv preprint arXiv:2501.12948*, 2025.

Wes Gurnee and Max Tegmark. Language models represent space and time. *arXiv preprint arXiv:2310.02207*, 2023.

David Ha, Andrew M Dai, and Quoc V Le. Hypernetworks. In *International Conference on Learning Representations*, 2017.

Danijar Hafner, Kuang-Huei Lee, Ian Fischer, and Pieter Abbeel. Deep hierarchical planning from pixels. In *Advances in Neural Information Processing Systems*, 2022.

Danijar Hafner, Jurgis Pasukonis, Jimmy Ba, and Timothy Lillicrap. Mastering diverse control tasks through world models. *Nature*, 2025.

Jean Harb, Pierre-Luc Bacon, Martin Klissarov, and Doina Precup. When waiting is not an option: learning options with a deliberation cost. In *Proceedings of the AAAI Conference on Artificial Intelligence*, 2018.

Geoffrey E Hinton and Drew van Camp. Keeping the neural networks simple by minimizing the description length of the weights. In *Proceedings of the Sixth Annual Conference on Computational Learning Theory*, 1993.

Edward J. Hu, yelong shen, Phillip Wallis, Zeyuan Allen-Zhu, Yuanzhi Li, Shean Wang, Lu Wang, and Weizhu Chen. LoRA: low-rank adaptation of large language models. In *International Conference on Learning Representations*, 2022.

Erik Jenner, Shreyas Kapur, Vasil Georgiev, Cameron Allen, Scott Emmons, and Stuart J Russell. Evidence of learned look-ahead in a chess-playing neural network. *Advances in Neural Information Processing Systems*, 2024.

Yiding Jiang, Evan Liu, Benjamin Eysenbach, J Zico Kolter, and Chelsea Finn. Learning options via compression. *Advances in Neural Information Processing Systems*, 2022.

Jared Kaplan, Sam McCandlish, Tom Henighan, Tom B Brown, Benjamin Chess, Rewon Child, Scott Gray, Alec Radford, Jeffrey Wu, and Dario Amodei. Scaling laws for neural language models. *arXiv preprint arXiv:2001.08361*, 2020.

Adam Karvonen. Emergent world models and latent variable estimation in chess-playing language models. In *Conference on Language Modeling*, 2024.

Taesup Kim, Sungjin Ahn, and Yoshua Bengio. Variational temporal abstraction. *Advances in Neural Information Processing Systems*, 2019.

Diederik P Kingma and Max Welling. Auto-encoding variational Bayes. *International Conference on Learning Representations*, 2014.

Thomas Kipf, Yujia Li, Hanjun Dai, Vinicius Zambaldi, Alvaro Sanchez-Gonzalez, Edward Grefenstette, Pushmeet Kohli, and Peter Battaglia. Compile: compositional imitation learning and execution. In *International Conference on Machine Learning*, 2019.

Seijin Kobayashi, Yassir Akram, and Johannes von Oswald. Weight decay induces low-rank attention layers. In *Advances in Neural Information Processing Systems*, 2024.

Yann LeCun. A path towards autonomous machine intelligence version 0.9. 2, 2022-06-27. *Open Review*, 2022.

Kenneth Li, Aspen K Hopkins, David Bau, Fernanda Viégas, Hanspeter Pfister, and Martin Wattenberg. Emergent world representations: exploring a sequence model trained on a synthetic task. In *International Conference on Learning Representations*, 2023.

Timothy P Lillicrap, Jonathan J Hunt, Alexander Pritzel, Nicolas Heess, Tom Erez, Yuval Tassa, David Silver, and Daan Wierstra. Continuous control with deep reinforcement learning. In *International Conference on Learning Representations*, 2016.

Scott W Linderman, Andrew C Miller, Ryan P Adams, David M Blei, Liam Paninski, and Matthew J Johnson. Bayesian learning and inference in recurrent switching linear dynamical systems. In *Proceedings of the 20th International Conference on Artificial Intelligence and Statistics, AISTATS 2017*, 2017.

Jack Lindsey, Wes Gurnee, Emmanuel Ameisen, Brian Chen, Adam Pearce, Nicholas L. Turner, Craig Citro, David Abrahams, Shan Carter, Basil Hosmer, Jonathan Marcus, Michael Sklar, Adly Templeton, Trenton Bricken, Callum McDougall, Hoagy Cunningham, Thomas Henighan, Adam Jermyn, Andy Jones, Andrew Persic, Zhenyi Qi, T. Ben Thompson, Sam Zimmerman, Kelley Rivoire, Thomas Conerly, Chris Olah, and Joshua Batson. On the biology of a large language model. *Transformer Circuits Thread*, 2025.

Kevin Meng, David Bau, Alex Andonian, and Yonatan Belinkov. Locating and editing factual associations in GPT. *Advances in Neural Information Processing Systems*, 2022.

Neel Nanda, Andrew Lee, and Martin Wattenberg. Emergent linear representations in world models of self-supervised sequence models. *arXiv preprint arXiv:2309.00941*, 2023.

Pedro A. Ortega, Jane X. Wang, Mark Rowland, Tim Genewein, Zeb Kurth-Nelson, Razvan Pascanu, Nicolas Heess, Joel Veness, Alex Pritzel, Pablo Sprechmann, Siddhant M. Jayakumar, Tom McGrath, Kevin Miller, Mohammad Azar, Ian Osband, Neil Rabinowitz, András György, Silvia Chiappa, Simon Osindero, Yee Whye Teh, Hado van Hasselt, Nando de Freitas, Matthew Botvinick, and Shane Legg. Meta-learning of sequential strategies. *arXiv preprint arXiv:1905.03030*, 2019.

Johannes von Oswald, Maximilian Schlegel, Alexander Meulemans, Seijin Kobayashi, Eyvind Niklasson, Nicolas Zucchet, Nino Scherrer, Nolan Miller, Mark Sandler, Blaise Agüera y Arcas, Max Vladymyrov, Razvan Pascanu, and João Sacramento. Uncovering mesa-optimization algorithms in transformers. *arXiv preprint arXiv:2309.05858*, 2023.

Koyena Pal, Jiuding Sun, Andrew Yuan, Byron C Wallace, and David Bau. Future lens: anticipating subsequent tokens from a single hidden state. *arXiv preprint arXiv:2311.04897*, 2023.

Kiho Park, Yo Joong Choe, and Victor Veitch. The linear representation hypothesis and the geometry of large language models. In *International Conference on Machine Learning*, 2024.

Shubham Pateria, Budhitama Subagdja, Ah-hwee Tan, and Chai Quek. Hierarchical reinforcement learning: a comprehensive survey. *ACM Computing Surveys (CSUR)*, 2021.

Bo Peng, Ruichong Zhang, Daniel Goldstein, Eric Alcaide, Xingjian Du, Haowen Hou, Jiaju Lin, Jiaxing Liu, Janna Lu, William Merrill, Guangyu Song, Kaifeng Tan, Saiteja Utpala, Nathan Wilce, Johan S. Wind, Tianyi Wu, Daniel Wuttke, and Christian Zhou-Zheng. RWKV-7 "Goose" with expressive dynamic state evolution. In *Conference on Language Modeling*, 2025.

Carsten Peterson. A mean field theory learning algorithm for neural network. *Complex Systems*, 1987.

Danilo Jimenez Rezende, Shakir Mohamed, and Daan Wierstra. Stochastic backpropagation and approximate inference in deep generative models. In *International Conference on Machine Learning*, 2014.

Jürgen Schmidhuber. *Making the world differentiable: on using self supervised fully recurrent neural networks for dynamic reinforcement learning and planning in non-stationary environments*. Inst. für Informatik, 1990.

Jürgen Schmidhuber. On learning to think: algorithmic information theory for novel combinations of reinforcement learning controllers and recurrent neural world models. *arXiv preprint arXiv:1511.09249*, 2015.

John Schulman, Philipp Moritz, Sergey Levine, Michael Jordan, and Pieter Abbeel. High-dimensional continuous control using generalized advantage estimation. *arXiv preprint arXiv:1506.02438*, 2015.

John Schulman, Filip Wolski, Prafulla Dhariwal, Alec Radford, and Oleg Klimov. Proximal policy optimization algorithms. *arXiv preprint arXiv:1707.06347*, 2017.

Richard S Sutton. Dyna, an integrated architecture for learning, planning, and reacting. *ACM Sigart Bulletin*, 1991.

Richard S Sutton, Doina Precup, and Satinder Singh. Between MDPs and semi-MDPs: a framework for temporal abstraction in reinforcement learning. *Artificial Intelligence*, 1999.

Mohammad Taufeeque, Philip Quirke, Maximilian Li, Chris Cundy, Aaron David Tucker, Adam Gleave, and Adrià Garriga-Alonso. Planning in a recurrent neural network that plays sokoban. *arXiv preprint arXiv:2407.15421*, 2024.

Emanuel Todorov, Tom Erez, and Yuval Tassa. Mujoco: a physics engine for model-based control. In *IEEE/RSJ International Conference on Intelligent Robots and Systems*, 2012.

Alexander Matt Turner, Lisa Thiergart, Gavin Leech, David Udell, Juan J Vazquez, Ulisse Mini, and Monte MacDiarmid. Steering language models with activation engineering. *arXiv preprint arXiv:2308.10248*, 2023.

Ashish Vaswani, Noam Shazeer, Niki Parmar, Jakob Uszkoreit, Llion Jones, Aidan N. Gomez, Lukasz Kaiser, and Illia Polosukhin. Attention is all you need. In *Advances in Neural Information Processing Systems*, 2017.

Johannes von Oswald, Nino Scherrer, Seijin Kobayashi, Luca Versari, Songlin Yang, Maximilian Schlegel, Kaitlin Maile, Yanick Schimpf, Oliver Sieberling, Alexander Meulemans, Rif A. Saurous, Guillaume Lajoie, Charlotte Frenkel, Razvan Pascanu, Blaise Agüera y Arcas, and João Sacramento. MesaNet: Sequence modeling by locally optimal test-time training. *arXiv preprint arXiv:2506.05233*, 2025.

Sang Michael Xie, Aditi Raghunathan, Percy Liang, and Tengyu Ma. An explanation of in-context learning as implicit Bayesian inference. In *International Conference on Learning Representations*, 2022.

Songlin Yang, Bailin Wang, Yikang Shen, Rameswar Panda, and Yoon Kim. Gated linear attention transformers with hardware-efficient training. In *International Conference on Machine Learning*, 2024a.

Songlin Yang, Bailin Wang, Yu Zhang, Yikang Shen, and Yoon Kim. Parallelizing linear transformers with the delta rule over sequence length. In *Advances in Neural Information Processing Systems*, 2024b.

Songlin Yang, Jan Kautz, and Ali Hatamizadeh. Gated delta networks: Improving Mamba2 with delta rule. In *International Conference on Learning Representations*, 2025.

Andy Zou, Long Phan, Sarah Chen, James Campbell, Phillip Guo, Richard Ren, Alexander Pan, Xuwang Yin, Mantas Mazeika, Ann-Kathrin Dombrowski, Shashwat Goel, Nathaniel Li, Michael J. Byun, Zifan Wang, Alex Mallen, Steven Basart, Sanmi Koyejo, Dawn Song, Matt Fredrikson, J. Zico Kolter, and Dan Hendrycks. Representation engineering: A top-down approach to AI transparency. *arXiv preprint arXiv:2310.01405*, 2023.

A ENVIRONMENT DETAILS

A.1 GRIDWORLD-PINPAD

Our grid world environment, referred to as gridworld-pinpad in the Appendix, is inspired by the previously proposed visual Pin Pad benchmark (Hafner et al., 2022). In our version, an agent is located in a grid world, together with uniquely colored cells (also referred to as objects). Within a task, the agent needs to step on a sequence of colored cells in a task-specific order.

A.1.1 MARKOV DECISION PROCESS SPECIFICATION

- **Task:** A task is specified by a sequence of colored cells to visit.
- **State:** The world is a 2D grid of size G-by-G. There are O unique colored cells placed on the grid, as well as W walls. At any given moment, the agent occupies one of the $G^2 - W$ cells that are not wall cells. Finally, the environment state also keeps track of what colored cells the agent has visited so far in the episode.
- **Action:** There are 4 actions corresponding to the 4 cardinal directions.
- **Dynamics:** Given the action and the agent position, the agent moves to the corresponding direction, except when it is moving towards a wall cell or outside of the grid, in which case the action results in a no-op. A colored cell is considered visited when the agent moves onto the cell from a different cell. If the agent successfully visits all colored cells in the right order, or if the agent visits a colored cell that is not the next cell specified by the task, or if the episode lasts longer than T steps, the episode ends.
- **Initial state:** At the beginning of every episode, the colored cells and walls, as well as the initial agent position are randomly sampled on the grid, ensuring there is no overlap.
- **Observation:** The agent's observation is the one-hot encoding of which object/wall is present in each cell, as well as the one-hot vector corresponding to the position of the agent, resulting in a $G^2(W + O + 1)$-dimensional vector.
- **Reward:** The agent gets a reward of 1 when successfully completing the task, and 0 otherwise.

A.1.2 TASK SPECIFICATION AND HYPERPARAMETERS

For both pretraining and post-training tasks, we use $G = 7$, $O = 8$, $W = 4$, and $T = 100$.

Numbering the colors from 0 to 7, the list of pretraining tasks can be found in Table A1. In this setup, the abstract subgoals combined to comprise the compositional final tasks, are given by $0 - 1$, $2 - 3$, $4 - 5$, and $6 - 7$.

We choose the post-training task to be $0 - 1 - 2 - 3 - 4 - 5 - 6 - 7 - 0 - 1 - 2 - 3$.

A.2 ANT-PINPAD

Ant-pinpad is a continuous control counterpart of the aforementioned gridworld-pinpad. The agent controls the classic MuJoCo ant (Schulman et al., 2015), with the goal of stepping on a sequence of colored cells in a task-specific order.

A.2.1 MARKOV DECISION PROCESS SPECIFICATION

- **Task:** A task is specified by a sequence of colored cells to visit.
- **State:** The state is a 2D plane, divided into grids. The grid is organized identically to that of the gridworld-pinpad, and also includes colored cells and walls. The state is further augmented by the proprioception state of the ant, as well as the precise coordinate of the center of the ant in the grid. Finally the environment state also keeps track of what colored cells the agent has visited so far in the episode.
- **Action:** The action is an 8-dimensional continuous vector representing the torque applied to the ant's eight joints.

0-1-4-5-0-1
0-1-4-5-2-3
0-1-6-7-2-3
2-3-0-1-4-5
2-3-6-7-2-3
2-3-6-7-4-5
4-5-0-1-4-5
4-5-0-1-6-7
4-5-2-3-6-7
6-7-2-3-0-1
6-7-2-3-6-7
6-7-4-5-0-1
0-1-6-7-4-5
2-3-0-1-6-7
4-5-2-3-0-1
6-7-4-5-2-3

Table A1: **Pretraining tasks for gridworld-pinpad.** Each $c_0 - ... - c_L$ list entry indicates a task consisting in visiting in order the colors c_0, $c_1 \dots c_L$ for some length L.

- **Dynamics:** Given the action, the ant moves on the 2D plane as usual. When the center of the ant enters a wall cell or whenever the vertical position of the ant's torso falls outside the valid operational range of $[0.2,\ 1.0]$, an episode is instantly terminated. A colored cell is considered visited when the ant enters the cell from a different cell. If the agent successfully visits all colored cells in the right order, or if the agent visits a colored cell that is not the next cell specified by the task, or when the episode lasts longer than T timesteps, the episode ends.
- **Initial state:** At the beginning of every episode, the colored cells and walls, as well as the initial agent position are randomly sampled on the grid, ensuring there is no overlap. We initialize the agent's full MuJoCo state by first setting the torso's x, y position in the plane to the center of the sampled grid cell. Then we add uniform noise that positions the agent in the simulation anywhere within the boundaries of the initial grid cell. We furthermore sample a random yaw-rotation and turn the agent correspondingly. Finally, the initial angles for all joints and initial velocities are sampled uniformly at random within a small range of 0.1 units around zero.
- **Observation:** The observation consists of the usual proprioception senses of the ant (to which the symlog function was applied, to ensure no excessively large values occur), concatenated with the global x, y ant coordinate (normalized to be between -1 and 1), as well as the relative position of the various colored cells and walls w.r.t. the ant, and the local coordinate of the ant within the current cell.
- **Reward:** The agent gets a reward of 1 when the task is successfully completed, and 0 otherwise.

A.2.2 Task specification and hyperparameters

For both pretraining and post-training tasks, we use $G = 4$, $O = 4$, $W = 1$, and $T = 500$.

The set of pretraining tasks can be found in Table A2.

We choose the post-training task to be $0 - 1 - 2 - 3$.

B Additional experimental results

B.1 Belief state probing

To determine whether the internal activations of the pretrained autoregressive models learn to identify temporal abstractions related to the subgoals, we analyze the internal activations of the models

0-3-2
1-0-3
2-1-0
3-2-1
0-2-0
0-2-1
0-3-1
1-0-2
1-3-1
1-3-2
2-0-2
2-0-3
2-1-3
3-1-0
3-1-3
3-2-0

Table A2: **Pretraining tasks for ant-pinpad.** Each $c_0 - \ldots - c_L$ list entry indicates a task consisting in visiting in order the colors c_0, $c_1 \ldots c_L$ for some length L.

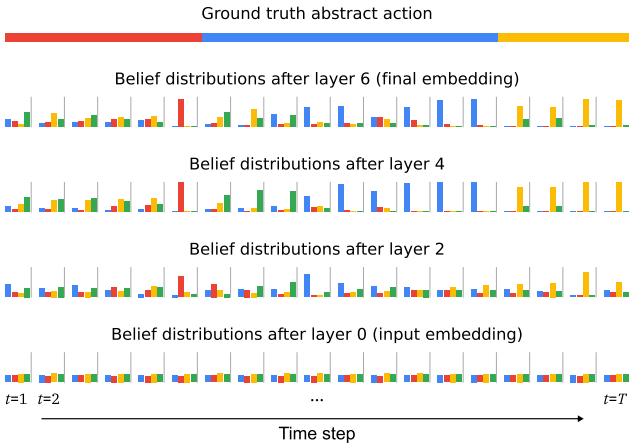

Figure A1: **Internal belief distributions over abstract actions, according to a linear probe.** Decoding performance of linear classifiers trained to predict groundtruth abstract actions from instantaneous residual stream activation vectors increases until mid-depth (layer 4) and remains strong up until the final embedding vector $e_{t,L}$ (here $L = 6$).

using linear probing (Alain & Bengio, 2017). To do so, we train linear classifiers to decode the agent subgoals $g_t \in \{1, \ldots, G\}$ on the grid world environment from the instantaneous (time step t) residual stream activation vector $e_{l,t} \in \mathbb{R}^{n_e}$ after the l-th model block (for further implementation details see Section C.2). Fig. A1 shows that linear decoder probability mass concentrates on the correct latent subgoal as time t increases, i.e. as more evidence about the current agent subgoal is gathered. Moreover, linear decoding likelihood increases with layer depth l, peaking close to the final embedding used by the transformer decoder. Fig. A2 quantitatively verifies these results. Moreover, comparing the performance of probes plugged into base models trained for a varying number of steps (x-axis), Fig. A2 reveals that while longer pretraining initially yields better internal representations excessive overtraining ultimately deteriorates the performance of subsequently trained linear controllers (especially those plugged in close to the output–layer 6–of the base odel).

To summarize, despite being trained only on one-step action prediction, the autoregressive models learn to represent temporally-abstract subgoals. This result is in line with the infinite-data theory of in-context Bayesian inference in sequence predictors (Ortega et al., 2019), and adds more evidence to the linear representation hypothesis in neural sequence models (Nanda et al., 2023; Park et al., 2024; Gurnee & Tegmark, 2023).

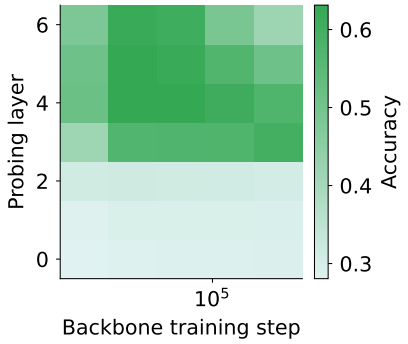

Figure A2: **Belief state probing at different network layers and base model training steps.** The latent goals governing the behavior of the data forced through a frozen pretrained sequence model become linearly decodable from residual stream activations deep in the network. Here, we display the final accuracy of linear probes trained to predict the latent goals from the residual stream activations of a frozen 6 layer transformer. We vary the training steps of the backbone and the layer at which the probe is plugged into the sequence model and report the mean performance over 10 backbone seeds.

B.2 Effect of controller depth on the steering capabilities of linear controllers

As a second test for the quality of internal representations, we perform causal model intervention (Geiger et al., 2021; Meng et al., 2022) and ask whether the internal representations of the autoregressive model can be leveraged to create a subgoal-optimizing policy. Inspired by the effectiveness of LoRA finetuning (Hu et al., 2022), we introduce a low-rank linear residual stream controller with parameters $U \in \mathbb{R}^{n_e \times n_e}$, which modifies the instantaneous residual stream activations in between model blocks at a given depth l following the update

$$e_{t,l} \leftarrow e_{t,l} + U_t e_{t,l}. \tag{4}$$

Note that we allow the controller parameters U_t to vary in time. In this section, we maintain a set of G separate controllers $\{U^{(g)}\}_{g=1}^{G}$, one per subgoal, and manually select which controller U_t to apply at every time step t using the groundtruth subgoal label g_t. To train the controllers, we condition generation upon the correct subgoal-specific controller $U^{(g)}$, and minimize the cross-entropy $\sum_{(o_{1:T+1},a_{1:T})\sim D_*} \sum_t -\ln p_{\theta,\phi}(a_t|o_{1:t}, g_t)$ w.r.t. controller parameters ϕ (while holding θ

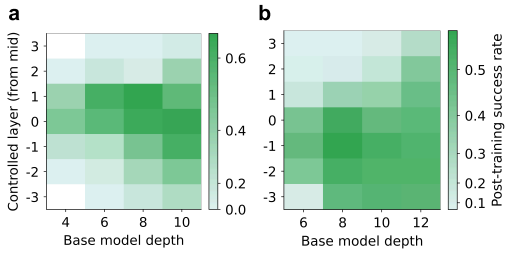

Figure A3: **Mid-depth linear internal controllers achieve length and compositional generalization.** Both panels analyze success rate (the fraction of rewarded trials in which the full sequence of elementary goals defining a given task is completed) as a function of base model depth (the number of autoregressive model layers) and controlled layer (the layer at which the internal controller is inserted, with 0 corresponding to the middle of the base model). In both grid world (**a**) and ant (**b**) environments, inserting the controller near the middle layer results in better controllability, as measured by the success rate on the post-training tasks, which require both length and compositional generalization. To produce this analysis, we trained one controller per subgoal using groundtruth labels; to evaluate success rates we activated the controllers in correct order, again using groundtruth subgoal labels. Results averaged over 5 seeds.

fixed) on a behavioral dataset D_*. This dataset contains behavioral sequences that are generated in the same way as those in the pretraining dataset D, but with increased optimality, see Section C.4.4. Here and throughout, ϕ refers to controller parameters that were not part of the pretrained model p_θ, and $p_{\theta,\phi}$ denotes a controlled model (for more implementation details see Section C.3).

We evaluate the subgoal-optimizing controllers on a post-training OOD task set that requires both length and compositional generalization: as shown in Fig. 2 and detailed in Appendix A, the post-training tasks recombine subgoals in orders not seen neither during pretraining nor controller training. As well, they comprise longer subgoal trajectories. Fig. A3 shows that these novel tasks can be solved with a high success rate by simply activating the corresponding subgoal controllers in the correct order, without any autoregressive sequence model retraining. We analyze the effect of hyperparameters of the base model pretraining on the just described controllability of internal representations in the next section (Section B.3).

B.3 Effect of sequence model training hyperparameters on the abstract action representations

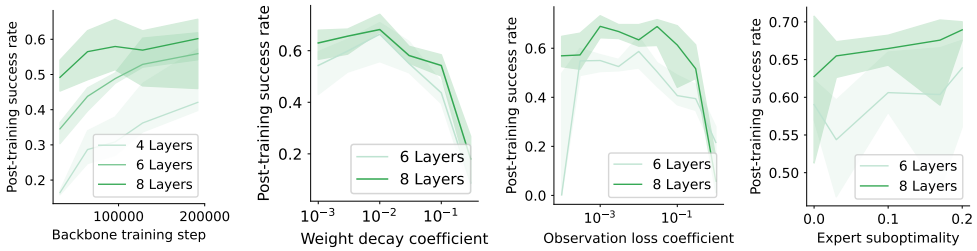

Figure A4: **Effect of sequence model training step (left), weight decay (center left), auxiliary observation loss (center right), and expert suboptimality ϵ (right) during pretraining on the controllers' compositional generalization.** The solid line represents the median performance over 10 runs, 1 seed for each of the 10 pretrained models, and the shaded area indicates the spread between the 25^{th} and 75^{th} quantiles.

In this section, we investigate the effect of various hyperparameter choices during sequence model training on the internal abstract action representation of the base autoregressive model. For all experiments, we use the gridworld-pinpad environment. We measure the quality of abstract action representation following the procedure outlined in Section C.3, and by evaluating the compositional generalization of the obtained controllers on post-training tasks. For all experiments, we use the same hyperparameters as detailed in Section C.3, unless specified otherwise. The results are presented in Fig. A4.

Sequence model training steps. For all base autoregressive model depths (4,6 and 8), we notice that longer sequence model training generally leads to better internal abstract action representation, such that the controllers generalize better to the post-training task set.

Sequence model training weight decay. For all base autoregressive model depths, we notice that weight decay during sequence model training is beneficial for internal representation. Interestingly, too much weight decay also degrades the representation, which points to a critical regularization trade-off that has been previously reported in foundation models (Kobayashi et al., 2024).

Observation auxiliary loss. Next, we observe that some amount of auxiliary loss (i.e. training to predict the next observation as well as action) is beneficial to building internal abstract action representation. With very low coefficient for the auxiliary loss, we noticed that some models completely failed to learn the representation; however we suspect this behavior is an artifact of our particular environment rather than a general trend.

Expert suboptimality. Finally, we investigate the effect of the suboptimality of the demonstrations used during pretraining on the resulting abstract action representation. We achieve this by

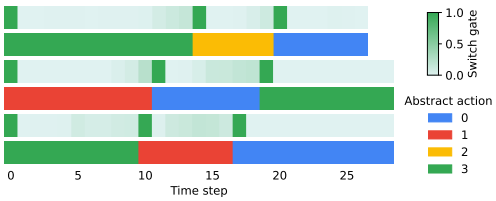

Figure A5: **Self-supervised metacontroller discovers temporally-abstract actions, gridworld-pinpad.** Three example trajectories from the gridworld-pinpad control environment showing the switch β_t used for temporal integration at each timestep, and the groundtruth abstract action being performed (color-coded). Switching ($\beta_t \approx 1$) coincides with a change in the abstract action being performed.

replacing the expert policy by an ϵ-noisy one, where at every timestep, with probability ϵ, a random (non terminating) action is taken. We see that the abstract action representation is robust against such suboptimality.

B.4 Unsupervised abstract action discovery

B.4.1 Temporal abstraction in the gridworld

In Fig. A5, we analyze the temporal abstraction discovered in the gridworld-pinpad setting (c.f. Fig. 3 for the respective ant-pinpad results), by plotting the switching gate values β_t against groundtruth abstract actions g_t. Similarly to the ant-pinpad setting, we find that the metacontroller essentially recovers the groundtruth abstract actions by the switch gate learning to behave in a quasi-binary fashion.

B.4.2 Quality of abstract actions

Figures A5 and 3 reveal that the temporal abstractions discovered by the metacontroller during self-supervised learning reflect the ground truth structure of the underlying task. In particular, the switching unit aligns with compositional abstract subgoals governing the observed data in a quasi-discrete fashion.

In this section, we focus instead on the controller latent code z, and provide evidence that the latent space encodes the actual subgoal-seeking abstract actions that constitute the compositional task, in a context-agnostic manner. To achieve this, we focus on the ant-pinpad environment, and follow the following procedure:

1. For a handful of grid configurations, we first perform an unconditioned rollout, i.e. a rollout in the environment using the sequence model and the trained metacontroller while sampling the z from the Gaussian prior, instead of the variational distribution.
2. Next, for each object, we consider unconditioned rollout trajectories that correspond to the agent visiting that object (and nothing else), and collect the latent codes z that were active at the time of visit. We hypothesize these latent codes to encode the subgoal seeking abstract action towards the corresponding object.
3. Finally, we use those latent codes in different scenarios, and demonstrate that the same latent code's subgoal seeking property generalizes to other situations.

Generalization to new configurations and switching timing Here, we investigate the ability of the latent code to generalize to new grid configurations and unseen switching times. The metacontroller is trained on successful, nearly-optimal trajectories where agents rarely demonstrate "backtracking" – behavior where an agent turns away from one object to seek another. Consequently, it is non-trivial whether a latent code injected mid-rollout can override the base model's current trajectory. As shown in Fig. A6, injecting a "go to blue" latent code at timestep 30 causes the agent to immediately correct its course, even if it was previously moving toward a different object. This intervention increases the goal-reaching success rate from 23% in the uncontrolled baseline to 36%.

This is significant, considering that the latent codes were generated for different configurations and are the result of a noisy sampling.

Generalization to out of distribution sequences We further test whether these codes can force behavior that is explicitly absent from the training data. In the ant-pinpad environment, the agent is never trained to seek object 1 immediately after object 0 (c.f. Section A). By manually activating the latent code for object 1 after the agent reaches object 0, we find the success rate for this OOD transition rises from 10% (baseline) to 24%. Note that this also tests whether the same latent codes can generalize to a new position in the sequence, since they were collected from trajectories where the ant visited the corresponding object as the first object.

Ultimately, these results indicate that the metacontroller does not merely learn to segment time, but successfully discovers a compact, steering-capable representation of functional intent—providing the necessary 'options' for internal RL to perform efficient credit assignment in complex, hierarchical tasks.

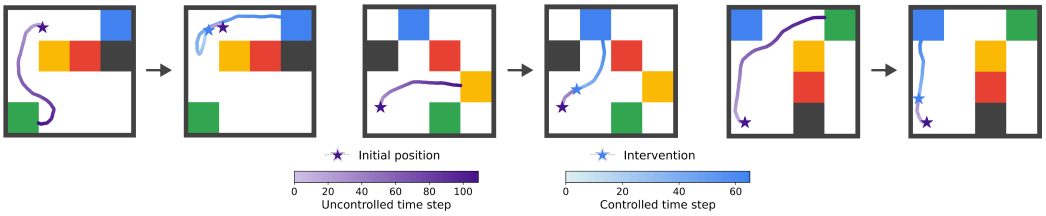

Figure A6: **Controller latent codes implement abstract actions.** Here, we illustrate the effect of a latent controller code implementing the abstract action "go to blue" in ant-pinpad, when forcing a switch at an arbitrary time. The three pairs display a trajectory without intervention by the metacontroller (left) vs. the one with the metacontroller running on a latent code corresponding to "go to blue" (right) respectively. The same controller latent code successfully steers the ant towards the desired color in different context, and regardless of the timing at which it is activated. Some trajectories demonstrate backtracking behavior when the control is applied.

B.5 Internal reinforcement learning

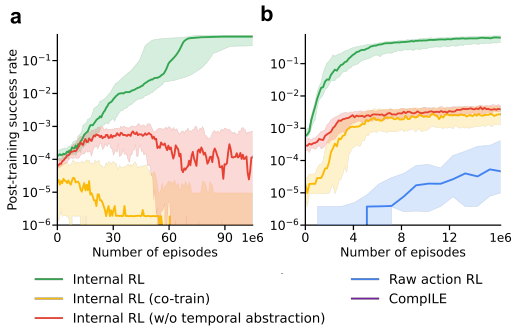

Figure A7: **Internal reinforcement learning solves sparse-reward compositional tasks where standard methods fail.** While some baselines see non-zero success rates at some time during RL training they fail to translate these successes into a policy maximizing reward. In turn, internal RL manages to successfully optimize the reward throughout training.

We complement the main text Fig. 4 by showing the same plot in log scale in Fig. A7. First, we notice that our internal RL methods achieves the highest success rate at the beginning of training, indicating that noise injection in the residual stream is useful for exploration, compared to exploration done by sampling raw actions alone. At the same time, despite their high initial success rate, the baselines completely fail at exploiting the experience to reinforce their success. This indicates that proper temporal abstraction is beneficial not only for exploration, but also exploitation as well.

C EXPERIMENTAL DETAILS

Here, we describe the details of training the sequence models (cf. Appendix D.1) as well as several variations of the controller (cf. Appendix D.2) acting on the then fixed sequence models to produce the results demonstrated in this paper. Moreover, in the final subsection we report the hyperparameters for each experiment.

C.1 PRETRAINING OF SEQUENCE MODELS

As a prerequisite for the main experiments that all involve tampering with the activations of a pretrained model, the base sequence models f_θ are first trained to autoregressively predict next actions a_t and next observations o_{t+1} given a sequence of observations $o_{1:t}$, on a set of meaningful expert trajectories. The details of the expert trajectory generation and sequence model training are given in the following.

C.1.1 EXPERT TRAJECTORY GENERATION

Given an environment and a set of pretraining tasks, expert trajectories are a set of corresponding successful trajectories. The trajectories are not necessarily optimal.

For the gridworld-pinpad environment, we analytically solve (via dynamic programming) for the stochastic policy that solves the shortest path problem, and, at every timestep, replace the action by a random (non terminating) action with probability ϵ. For all results unless explicitly specified, we chose $\epsilon = 0$, but show the robustness against such noise in Section B.3.

For the ant-pinpad environment, we obtain the expert trajectories by training an RL agent. In order to train a single agent for the different task, we augment the observation in the following way: for each cell of the grid, the agent is given an additional 4-dimensional 1-hot vector, indicating one of the 4 cardinal directions the agent must move towards to follow the shortest path at the grid-level. Furthermore, an additional intrinsic reward corresponding to the dot product between the agent's velocity and this direction is given. The agent is trained by PPO Schulman et al. (2017), see Table A3 for the hyperparameters used.

Note that the resulting expert trajectories are not always successful. The success rate for the pretraining tasks is at 0.8, and for the post-training tasks at 0.7. The success rate in Figure 4 is normalized by this score.

Table A3: Hyperparameters for expert training on the ant-pinpad environment.

Hyperparameter	**Search**
Embedding dimension n_e	256
Backbone model	SSM
Backbone model depth	6
Train steps	256000
Batch size	1024
Optimizer	AdamW
Learning rate	[3e-4]
Weight decay	[0.03]
Entropy reg	[0.0003]
βs	(0.9, 0.999)
Scheduler	Constant learning rate

C.1.2 SEQUENCE MODEL TRAINING

Given a dataset D of expert trajectories, the sequence models are trained to maximize the log-likelihood of the data

$$\begin{aligned}&\max_{\theta} \log \prod_{(o_{1:T+1}, a_{1:T}) \sim D} \prod_{t=1}^{T} p_\theta(a_t|o_{1:t}) p_\theta(o_{t+1}|o_{1:t}) \\ &= \max_{\theta} \sum_{(o_{1:T+1}, a_{1:T}) \sim D} \sum_{t=1}^{T} \log p_\theta(a_t|o_{1:t}) + \log p_\theta(o_{t+1}|o_{1:t}).\end{aligned} \tag{5}$$

Switching the sign and reweighting the observation component with a coefficient λ yields the loss function presented in the main text, repeated below for convenience:

$$\begin{aligned}\min_{\theta} L(\theta) = \min_{\theta} \sum_{(o_{1:T+1}, a_{1:T}) \sim D} \sum_{t=1}^{T} &- \log p_\theta(a_t|o_{1:t}) \\ &- \lambda \log p_\theta(o_{t+1}|o_{1:t}).\end{aligned} \tag{6}$$

Table A4 summarizes the hyperparameter choices for training sequence models on the discrete gridworld and Table A5 those for the ant. For the sequence models, we use the hyperparameters specified in Table A15 for SSMs and those specified in Table A16 for transformers. We use SSMs for the ant-pinpad and transformers in the gridworld-pinpad.

Table A4: Hyperparameters for sequence model training on the gridworld environment.

Hyperparameter	**Search**
Embedding dimension n_e	256
Backbone model	Transformer
Backbone model depth	6
Observation coefficient λ	[0, 0.01]
Train steps	256000
Batch size	1024
Optimizer	AdamW
Learning rate	[3e-4]
Weight decay	[0.03]
βs	(0.9, 0.999)
Scheduler	Constant learning rate

Table A5: Hyperparameters for sequence model training on the ant-pinpad environment.

Hyperparameter	**Search**
Embedding dimension n_e	256
Backbone model	SSM
Backbone model depth	8
Observation coefficient λ	10
Train steps	204800
Batch size	512
Optimizer	AdamW
Learning rate	3e-4
Weight decay	0.03
βs	(0.9, 0.999)
Scheduler	Constant learning rate

C.1.3 SEED

For both environments, we pretrain 10 such sequence models with different seeds.

C.2 BELIEF STATE PROBING

Given a pretrained sequence model f_θ optimized to maximize Equation 6, we train linear probes to predict the latent subgoals governing a sequence at hand. More formally, given a sensori-action sequence $(o_{1:T+1}, a_{1:T})$ we train a linear probe $U_l \in \mathbb{R}^{n_e, n_g}$ to predict the latent subgoal g_t from the residual activation $e_{t,l}$ at layer $l \in 0, ..., L$ at every timestep t. Here, n_e and n_g denote the residual stream dimension and total number of subgoals in the dataset respectively and L is the number of layers of f_θ. The belief distribution over the subgoals at timestep t is parameterized as

$$p(g_t = g|e_t) = \text{softmax}(U_l e_{t,l})_g. \tag{7}$$

The parameters U_l are trained to minimize the cross-entropy loss

$$L(U_l) = \sum_{(o_{1:T+1}, g_{1:T}) \sim D} \sum_{t=1}^{T} -\log p(g_t|e_{1:t,l}) \tag{8}$$

Table A6 summarizes the hyperparameter choices for these experiments.

Table A6: Hyperparameters for belief state probing in gridworld.

Hyperparameter	**Search**
Embedding dimension n_e	256
Backbone train steps	[16K, 32K, 64K, 128K, 256K]
Probe layers	[0, 1, 2, 3, 4, 5, 6]
Train steps probe	8000
Batch size	512
Optimizer	AdamW
Learning rate	[1e-3]
Weight decay	[0.0]
βs	(0.9, 0.999)
Scheduler	Constant learning rate

C.3 CONTROLLER COMPOSITIONAL GENERALIZATION

Given a pretrained and subsequently fixed sequence model f_θ, a modification of the metacontroller c_ϕ as defined in Appendix D.2 is inserted into the base autoregressive model at some layer $l \in 0, ..., L$. Here, L is the total number of layers of the base autoregressive model. The metacontroller used in these experiments deviates from the vanilla version in how the latent codes z_t are computed. Instead of sampling $\tilde{z}_t$ from a normal distribution and then temporally integrating according to

$$z_t = \beta_t \odot \tilde{z}_t + (1 - \beta_t) \odot z_{t-1}$$

$\beta_t = 1$ is forced for all t. Moreover, in these experiments, the ground truth information about abstract behaviour is injected via $\tilde{z}_t$. In particular, the expert trajectories $(o_{1:T+1}, a_{1:T})$ are annotated with the IDs of the abstract actions that governed the behavior during generation. Note that, contrary to the raw action a_t, the abstract action and hence the identifier ID_t provided to the metacontroller only change sparsely in time. Formally, given the ground truth labels, the controller latent code at time step t is given by

$$z_t = \tilde{z}_t = \text{onehot}(\text{ID}_\text{t}, K),$$

the onehot encoding of ID_t. Here, K denotes the total number of unique abstract actions in the dataset $\mathcal{D}$. With access to this additional privileged information, we train the parameters ϕ to further maximize the data log-likelihood (cf. Equation 6).

Table A7 summarizes the hyperparameter choices for the controller compositional generalization on the discrete gridworld and Table A8 those for the ant.

C.4 UNSUPERVISED ABSTRACT ACTION DISCOVERY

Given a pretrained, frozen base sequence model f_θ, the metacontroller c_ϕ as described in Appendix D.2 is inserted into the base model at some layer $l \in 0, ..., L$ where L is the base model

Table A7: Hyperparameters for the controller compositional generalization experiment on the gridworld environment.

Hyperparameter	**Search**
Observation coefficient λ	0
Controller model	Low-rank (16) linear
Controlled layer l	$L/2$
Train steps	3200
Batch size	512
Optimizer	AdamW
Learning rate	[1e-3]
Weight decay	[0.03]
βs	(0.9, 0.999)
Scheduler	Constant learning rate

Table A8: Hyperparameters for the controller compositional generalization experiment on the ant-pinpad environment.

Hyperparameter	**Search**
Observation coefficient λ	0
Controller model	Linear
Controlled layer l	$L/2$
Train steps	3200
Batch size	256
Optimizer	AdamW
Learning rate	[3e-4]
Weight decay	[0.03]
βs	(0.9, 0.999)
Scheduler	Constant learning rate

depth. With θ frozen, the metacontroller parameters ϕ are trained to (further) minimize a regularized NLL. Note that the metacontroller c_ϕ learns to generate and make use of an acausal embedding $s(e_{1:T})$. Thus, by controlling the base model, the metacontroller can minimize the NLL beyond the loss-level attained by the causal base autoregressive model. Beyond optimizing Equation 6, the posterior over controller latent codes

$$\tilde{z}_t \sim \mathcal{N}(z_{\text{enc}}; \mu_t, \Sigma_t)$$

is regularized so that at test time meaningful controller latent codes can be sampled from the prior $\mathcal{N}(0, I)$. To allow this, the Kullback-Leibler divergence between both distributions

$$D_{\text{KL}}\big(\mathcal{N}(\mu_t, \Sigma_t) \,\|\, \mathcal{N}(0, I)\big) \tag{9}$$

is added to the NLL objective. Putting everything together, and adding regularization strength α the metacontroller c_ϕ is trained to minimize the loss

$$\begin{aligned} L(\phi) = \sum_{(o_{1:T+1}, a_{1:T}) \sim D} \sum_{t=1}^{T} & - \log p_{\phi,\theta}(a_t | o_{1:t}) \\ & - \lambda \log p_{\phi,\theta}(o_{t+1} | o_{1:t}) \\ & + \alpha D_{\text{KL}}\big(\mathcal{N}(\mu_t, \Sigma_t) \,\|\, \mathcal{N}(0, I)\big) \end{aligned} \tag{10}$$

where $p_{\phi,\theta}$ denotes the probability computed by the sequence model f_θ when controlled by c_ϕ. This objective is motivated as the evidence lower bound (ELBO) in Section E.1. Again, note that only the parameters ϕ are trained while the sequence model θ remains frozen.

The hyperparameters for training the metacontroller in gridworld- and ant-pinpad are summarized in Table A9 and Table A10, respectively.

Table A9: Hyperparameters for unsupervised abstract action discovery on the gridworld environment.

Hyperparameter	**Search**
Observation coefficient λ	0
KL strength α	[0, 0.05, 0.1, 0.17, 0.3, 0.5, 1]
Controller model	Low-rank (16) linear
Controlled layer l	$L/2$
Latent code dimension n_z	8
Controller encoder hidden layer	64
Controller decoder hidden layer	32
GRU dimension n_h	32
Sequence embedding dimension n_s	32
Train steps	64000
Batch size	512
Optimizer	AdamW
Learning rate	[1e-3]
Weight decay	[0.03]
βs	(0.9, 0.999)
Scheduler	Constant learning rate

Table A10: Hyperparameters for unsupervised abstract action discovery on the ant-pinpad environment.

Hyperparameter	**Search**
Observation coefficient λ	0
KL strength α	[0, 0.05, 0.1, 0.17, 0.3, 0.5, 1]
Controller model	Linear
Controlled layer l	$L/2$
Latent code dimension n_z	8
Controller encoder hidden layer	64
Controller decoder hidden layer	32
GRU dimension n_h	32
Sequence embedding dimension n_s	32
Train steps	32000
Batch size	128
Optimizer	AdamW
Learning rate	[3e-4]
Weight decay	[0.03]
βs	(0.9, 0.999)
Scheduler	Constant learning rate

C.4.1 BASELINE – FORCED RESETS

This baseline aims to answer the question whether a metacontroller not factorizing the controller latent code z_t into explicit subsequences via β_t discovers abstract actions suitable for subsequent internal RL. To do so, we perform the exact same experiment as described so far in this subsection with the only difference that $\beta_t = 1$ is forced at every timestep. Hence, z_t is equal to the latent controller code proposal $\tilde{z}_t$.

C.4.2 BASELINE – METACONTROLLER COTRAINING

This baseline investigates whether the two stage approach of first training the sequence model f_θ, freezing it, and only then training the metacontroller c_ϕ yields different results than cotraining both θ and ϕ. In this pursuit, we perform 2 experiments: for gridworld, no pretrained θ is assumed and instead both θ and ϕ are both randomly initialized and jointly trained to optimize the regularized NLL defined in Equation 3 (else used for training ϕ in a frozen f_θ). For ant-pinpad, θ is initialized to the pretrained parameter, but we still jointly train ϕ and θ to optimize the objective.

C.4.3 BASELINE – COMPILE

We adapted CompILE (Kipf et al., 2019; Jiang et al., 2022) as best as possible to our setting.

On a high level, CompILE is very similar to our cotraining baselines: it is a latent variable model (albeit with a different set of latent variables) which takes a sequence of observations and output, for each timestep, a continuous latent variable z drawn from a Gaussian that then condition a policy trained to imitate the action in the trajectory. Similarly to us, it is a variational inference approach to discovering the abstract actions, except that it does not leverage the internal representation of a pretrained model. CompILE also infers the switching latent variables β, and requires a prior distribution over the switching rate and the maximum number M of abstract actions (or segments) in all sequences.

To make things comparable, we adopt CompILE to our architecture by drop-in replacing the meta-controller by the CompILE module which generates the latent code z, while keeping everything else identical. In particular, the same sequence model architecture is used and internally controlled by z. Nevertheless, to remain close to the original architecture of CompILE, the module generating the latent code takes as input the raw input, instead of the residual stream activation. To compensate for the potential loss in expressivity, we use as the recurrent encoder of the module the same architecture as the first half of the sequence model. The parameters for the distribution of the latent variables are then generated by a one hidden layer MLPs with hidden dimension n_h. Due to the difficulty of performing parallel inference when using the algorithm, the sequence model parameters θ are initialized to the pretraining value, such that training can be shortened.

Table A11 (resp. A12) shows the hyperparameter used for gridworld (resp. ant-pinpad).

Table A11: Hyperparameters for CompILE training on the gridworld environment.

Hyperparameter	**Search**
MLP hidden dim n_h	32
Observation coefficient λ	0
KL strength for latent z α_z	[0.003, 0.01, 0.03, 0.1, 0.3, 1]
KL strength for latent β α_β	[0.003, 0.01, 0.03, 0.1, 0.3, 1]
Gumbel softmax temperature for β	[0.5, 1]
Maximum number of segments M	4
Prior switching rate	10
Controller model	Low-rank (16) linear
Controlled layer l	$L/2$
Latent code dimension n_z	8
Train steps	32000
Batch size	512
Optimizer	AdamW
Learning rate	[1e-3]
Weight decay	[0.03]
βs	(0.9, 0.999)
Scheduler	Constant learning rate

C.4.4 METACONTROLLER TRAINING DATASET

While our experiments reveal that the emergence of abstract actions in the sequence model is robust to suboptimality (c.f. Appendix B.3) the opposite holds for discovering these abstract actions in the frozen sequence model with the metacontroller. Empirically, we observe that as the demonstrations used for training the metacontroller get cleaner (i.e. the closer they resemble the optimal stochastic policy), the ability of the metacontroller to compress the abstract actions onto a latent space improves. Therefore, for training the metacontroller, for ant-pinpad, we generate trajectories by taking the mean of the Gaussian distribution generated by the expert for each timestep instead of sampling from it. Similarly, for grid we set the suboptimality degree $\epsilon = 0$, to obtain clean expert demonstration.

Table A12: Hyperparameters for CompILE training on the ant-pinpad environment.

Hyperparameter	**Search**
MLP hidden dim n_h	32
Observation coefficient λ	0
KL strength for latent z α_z	[0.003, 0.01, 0.03, 0.1, 0.3, 1]
KL strength for latent β α_β	[0.003, 0.01, 0.03, 0.1, 0.3, 1]
Gumbel softmax temperature for β	[0.5, 1]
Maximum number of segments M	4
Prior switching rate	10
Controller model	Linear
Controlled layer l	$L/2$
Latent code dimension n_z	8
Train steps	32000
Batch size	128
Optimizer	AdamW
Learning rate	[3e-4]
Weight decay	[0.03]
βs	(0.9, 0.999)
Scheduler	Constant learning rate

C.4.5 SEED

For all environments and methods, for each of the 10 pretrained sequence models and each of the hyperparameter configurations, we perform this unsupervised abstract action discovery over 3 different seeds.

C.5 RL EXPERIMENTS

C.5.1 INTERNAL RL

We present in algorithm 2 the initialization function for the internal RL environment, and 1 the effective internal RL environment step function, given the original environment, a pretrained base autoregressive model and corresponding meta controller. Algorithm 3 shows the full training loop.

The hyperparameters for training the agent in gridworld- and ant-pinpad are summarized in Table A13 and Table A14, respectively.

Table A13: Hyperparameters for internal RL on the gridworld environment.

Hyperparameter	**Search**
Policy model	SSM
Policy depth	1
Policy embedding dimension	256
Train steps	100000
Batch size	1024
Entropy regularizer	0
Optimizer	AdamW
Learning rate	[3e-5]
Weight decay	[0.0]
βs	(0.9, 0.999)
Scheduler	Constant learning rate

C.5.2 RL ALGORITHM DETAILS

For all RL experiments, we used an RL algorithm suitable for sparse, single final reward setting. The algorithm is related to the GRPO algorithm, except for the notion of group which is absent in our setting. Similarly to GRPO, we modify the standard Proximal Policy Optimization (PPO; Schulman

Algorithm 1: The effective internal RL environment step function

require: Original environment E, switching unit f_{switch}, controller decoder f_{hyp}, model blocks $f_{\text{block}_{:l}}$ up to layer l, model blocks $f_{\text{block}_{l:}}$ from layer l. The function takes the abstract action z, and the internal state s as inputs.

`step` (z, s):
- $\beta \leftarrow 0$
- done $\leftarrow$ False
- $r_{\text{acc}} \leftarrow 0$
- $(e, h_{\text{switch}}, h_{\text{block}_{l:}}, h_{\text{block}_{:l}}) \leftarrow s$
- **while** $\beta < \beta_{threshold}$ **do**
  - $U \leftarrow f_{\text{hyp}}(z)$
  - $a, h_{\text{block}_{l:}} \sim f_{\text{block}_{l:}}(e + Ue, h_{\text{block}_{l:}})$
  - $o, r,$ done $\sim E.\text{step}(a)$
  - $e, h_{\text{block}_{:l}} \leftarrow f_{\text{block}_{:l}}(o, h_{\text{block}_{:l}})$
  - $\beta, h_{\text{switch}} \leftarrow f_{\text{switch}}(e, z, h_{\text{switch}})$
  - $r_{\text{acc}} \leftarrow r_{\text{acc}} + r$
- $s \leftarrow (e, h_{\text{switch}}, h_{\text{block}_{l:}}, h_{\text{block}_{:l}})$
- **return** $(e, r_{acc}, done), s$

Algorithm 2: The internal RL initialization function

require: Original environment E, switching unit f_{switch}, controller decoder f_{hyp}, model blocks $f_{\text{block}_{:l}}$ up to layer l, model blocks $f_{\text{block}_{l:}}$ from layer l.

`init` ():
- $o, r,$ done $\sim E.\text{init}()$
- $h_{\text{block}_{l:}} \leftarrow f_{\text{block}_{l:}}.\text{init}()$
- $h_{\text{block}_{:l}} \leftarrow f_{\text{block}_{:l}}.\text{init}()$
- $h_{\text{switch}} \leftarrow f_{\text{switch}}.\text{init}()$
- $e, h_{\text{block}_{:l}} \leftarrow f_{\text{block}_{:l}}(o, h_{\text{block}_{:l}})$
- $\beta, h_{\text{switch}} \leftarrow f_{\text{switch}}(e, z, h_{\text{switch}})$
- $s \leftarrow (e, h_{\text{switch}}, h_{\text{block}_{l:}}, h_{\text{block}_{:l}})$
- **return** $(e, r, done), s$

Algorithm 3: The internal RL full algorithm

require: Policy π_θ

for *epoch* $e = 1 \ldots E$ **do**
- $\mathcal{B} \leftarrow []$
- **for** *batch element* $b = 1 \ldots B$ **do**
  - $(e, r, done), s \leftarrow$ `init`()
  - $h_\pi \leftarrow \pi_\theta.\text{init}()$
  - $\tau \leftarrow []$
  - **while** *not done* **do**
    - # acting on a temporally abstract timescale (see algorithm 1)
    - $z, h_\pi \sim \pi_\theta(e, h_\pi)$
    - $\tau.\text{append}((e, r, done, z))$
    - $(e, r, done), s \leftarrow$ `step`(z, s)
  - $\tau.\text{append}((e, r, done, None))$
  - $\mathcal{B}.\text{append}(\tau)$
- Update policy π_θ using $\mathcal{B}$ by maximizing the objective in Eq 11

Output π_θ

Table A14: Hyperparameters for internal RL on the ant-pinpad environment.

Hyperparameter	Search
Policy model	SSM
Policy depth	1
Policy embedding dimension	256
Train steps	51200
Batch size	256
Entropy regularizer	0
Optimizer	AdamW
Learning rate	[3e-5]
Weight decay	[0.0]
βs	(0.9, 0.999)
Scheduler	Constant learning rate

et al., 2017) framework by replacing the learned value function (critic) with an empirical advantage estimation.

Objective function. We optimize the policy by maximizing a clipped surrogate objective similar to PPO. The loss is defined as:

$$\mathbb{E}_\tau\Big[\sum_t \min(\frac{\pi_\theta(a_t|s_{1:t})}{\pi_{\theta_{\text{old}}}(a_t|s_{1:t})}, \text{clip}(\frac{\pi_\theta(a_t|s_{1:t})}{\pi_{\theta_{\text{old}}}(a_t|s_{1:t})}, 1-\epsilon, 1+\epsilon))\mathcal{A}_\tau\Big] \tag{11}$$

where π_θ is the current policy and $\pi_{\theta_{\text{old}}}$ is the previous policy, $\mathcal{A}_t$ is the relative advantage of the trajectory τ.

Relative advantage estimation. We adopt the critic-free approach to estimating the advantage.

The relative advantage $\mathcal{A}_\tau$ measures how much better (or worse) a specific trajectory τ is compared to the average quality of the entire batch of size B. It is calculated by normalizing the reward $R(\tau)$ relative to the batch's mean $\bar{R}$ and standard deviation σ_R:

$$\bar{R} = \frac{1}{B}\sum_{i=1}^{B} R(\tau_i)$$

$$\sigma_R = \sqrt{\frac{1}{B}\sum_{i=1}^{B}(R(\tau_i)-\bar{R})^2}$$

$$\mathcal{A}_\tau = \frac{R(\tau)-\bar{R}}{\sigma_R+\delta},$$

where δ is a small constant (e.g., 10^{-3}) to ensure numerical stability and prevent division by zero.

C.5.3 Baseline – raw action RL

For the raw action RL baseline, we simply use the pretrained sequence model without any metacontroller, and finetune it on the post-training task using the RL algorithms described in section C.5.2, in raw action space. Since for the raw action RL baseline, there is no unsupervised abstract action discovery phase, we instead do the RL over 3 seeds.

C.5.4 Baseline – others

For all other baselines, we simply perform internal RL with the respective metacontrollers obtained during the unsupervised abstract action discovery, cf section C.4.

C.5.5 SEED AND HYPERPARAMETER SELECTION

For each method, we scan over different learning rates $(0.000003, 0.00001, 0.00003, 0.0001, 0.0003)$ and pick the learning rate and hyperparameter configuration from the unsupervised abstract action discovery with the best median RL performance over the 10 pretrained model and 3 seed.

C.6 RATE-DISTORTION CURVE

The rate distortion curve is plotted after performing the unsupervised abstract action discovery with the same hyperparameters as described in section C.4, with the exception of using the Gumbel-Sigmoid trick for the switching units as derived in E.1 for gridworld-pinpad, as it resulted in a cleaner Pareto frontier. As the pretrained sequence models have each different Pareto frontier which would hide its structure, we pick one sequence model at random, and instead do the unsupervised abstract action training with 10 seeds on each of the different KL strength α. We do this for our method, as well as the metacontroller cotraining baseline.

The sum of switching value is computed by hard-thresholding the continuous switching value with $\beta_{\text{threshold}} = 0.5$ as we do in the internal RL (cf algorithm 1), and taking the average sum over trajectories. We manually checked the forget patterns to label whether the switching patterns aligned with the subgoal change.

D ARCHITECTURE DETAILS

D.1 SEQUENCE MODEL

We parametrize the base model as an autoregressively-trained multi-layer sequence model f_θ. The specific instantiations of f_θ detailed below utilize either standard transformer Vaswani et al. (2017) or recurrent neural network (also commonly referred to as state-space model, SSM) layers. From the latter family (Yang et al. (2024b;a; 2025); Beck et al. (2024); De et al. (2024); Gu & Dao (2024); Peng et al. (2025); von Oswald et al. (2025) and others), we choose the Hawk De et al. (2024) due to its simplicity and computational efficiency.

D.1.1 SSM

For SSM-based sequence models, we employ a standard pre-normalization layer architecture. Inputs are normalized before being fed into the recurrent Hawk sequence mixing block De et al. (2024), whose output is added back to the residual stream. This is followed by an MLP channel-mixing block that similarly applies normalization to its input before adding its output back to the residual stream.

Table A15: Hyperparameters for hawk state space model layers.

Hyperparameter	**Value**
Embedding dimension n_e	256
Hawk LRU dimension	256
Number of heads	8
Variance scaling of all initializers	0.1
MLP hidden layer dimension	512
MLP nonlinearity	ReLU

D.1.2 TRANSFORMER

For transformer-based models, we employ a standard pre-normalization layer architecture. We first compute relative position embeddings to serve as attention biases. Inputs are then normalized and fed into the Multi-Head Attention sequence mixing block (incorporating these biases), whose output is added back to the residual stream. This is followed by an MLP channel-mixing block that applies normalization to its input before adding its output back to the residual stream.

Table A16: Hyperparameters for transformer model layers.

Hyperparameter	Value
Embedding dimension n_e	256
Attention head dimension	64
Number of heads	4
Variance scaling of all initializers	0.1
MLP hidden layer dimension	512
MLP nonlinearity	ReLU
Number of buckets for relative positional encodings	32

D.2 METACONTROLLER ARCHITECTURE

Design principles. The metacontroller is designed to act inside a frozen, autoregressive sequence model backbone. It does so by modulating the residual stream activations at some backbone layer via simple, internal controllers. Manipulating the residual stream allows the metacontroller to implement temporally abstract actions that turn the sequence model into a subgoal-optimizing policy pursuing a selected goal over multiple raw action timesteps.

These temporally abstract actions implement the subgoals governing the behaviour of the agents whose trajectories constitute the offline data available for metacontroller training. To discover these abstract actions, the metacontroller tracks a recurrent latent variable z_t capturing the subgoal active at step t and then translates it into an action (linear controller). The true posterior $p(z_t|e_{1:T})$ over this latent z_t is inherently acausal since (sub)goals only materialize over an entire trajectory. To make this tangible consider an agent that is placed in the gridworld with the intent to "go to red". As the agent takes its first goal-directed actions, an outside observer will have a hard time determining the underlying goal since reaching other colored cells like green might require taking the very same first actions. Only as the action sequence further unfolds and the evidence of the agent's intent becomes conclusive the goal can be identified. These considerations underline that to correctly infer the subgoal at step t, in general, the metacontroller needs access to sequence-level information. They also reveal that the purely causal backbone is limited to, at best, discover a powerful online inference algorithm for latent subgoals.

Now, as is the case for real world data, assume that the offline trajectories include the behavior of agents completing subgoals and subsequently switching to new subgoals. It is desirable for the metacontroller to infer the latent z_t in a way that makes the factorization into subgoals accessible. This boils down to parameterizing z_t as a temporal composition of latent codes $\tilde{z}_t$ orchestrated by a switching unit $\beta_t \in [0, 1]$. Selecting $\beta_t \approx 1$ implements switching subgoals and, equally important to achieve temporally consistent behaviour, $\beta_t \approx 0$ allows to maintain the previous subgoal. While, as discussed above, the $\tilde{z}_t$ needs to be acausal, β_t is parameterized to be causal. This allows the metacontroller to identify when to switch goals at test time (when no acausal information is available). For more justification of this choice, see Section E.1.

High-level description. On a high level, the metacontroller c_ϕ (cf. Fig. A8) can be viewed as a recurrent hypernetwork (Ha et al., 2017). It acts inside a frozen sequence model backbone f_θ by emitting *internal, linear controllers* U_t altering the residual activations at timestep t. Architecturally, it is an encoder-decoder generative model that allows to sample controllers that, after training, implement abstract actions. First, at every timestep the recurrent *controller encoder* stochastically proposes controller latent codes $\tilde{z}_t$ conditioned on an acausal embedding $s(e_{1:T})$ generated by the *internal sequence embedder*. Also per timestep, the *switching unit* emits a temporal integration rate β_t. Subsequently, the *temporal integration unit* takes per timestep latent proposals and composes them sparsely in time by applying the temporal integration rate. The temporally integrated latent controller codes z_t are then mapped to instantaneous controllers by the *controller decoder*.

Architectural details. Adopting the standard design principles for sequence models, the pretrained sequence model f_θ is built from L stacked layers (cf. Appendix D.1). While processing the sequence of inputs $o_{1:T}$ to predict $(a_{1:T}, o_{2:T+1})$ the sequence model generates a sequence of residual stream activations $e_{1:T,l}$ at each layer $l \in \{0, ..., L\}$ (0 refers to the residual activations

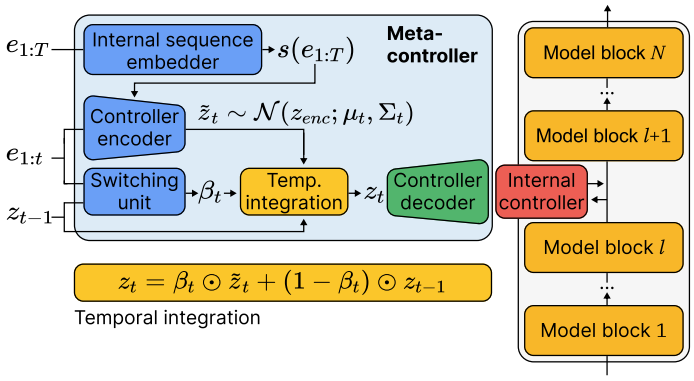

Figure A8: **Metacontroller architecture** (same as Fig. 2).

immediately before the first layer). The metacontroller operates inside the sequence model at layer l by reading these residual activations $e_{1:T,l}$ and applying an internal, linear controller

$$\hat{e}_{t,l} = e_{t,l} + U_t e_{t,l}. \tag{12}$$

This controlled residual activation $\hat{e}_{t,l}$ is passed to the subsequent model blocks, which are unaware of the intervention. The following details the metacontroller architecture used to learn these interventions from offline data.

The metacontroller keeps track of two summarizing states–a summary state h_t of the history of activations $e_{1:t,l}$ and an embedding $s(e_{1:T,l})$ summarizing the entire sequence of activations $e_{1:T}$. The history is generated by a GRU Cho et al. (2014) and compresses information from past residual activations in its n_h dimensional hidden state

$$h_t = \text{GRU}(e_t, h_{t-1}). \tag{13}$$

This hidden state allows the metacontroller to remember relevant information about the history at test-time. Beyond the history, as discussed above, the metacontroller needs access to sequence level (acausal) information to fulfill its overarching purpose to approximate the posterior $q(z_t|e_{1:T})$. This information is provided through the **internal sequence embedder** f_{emb}. It takes the trajectory of residual stream activations $e_{1:T,l}$ produced at layer l and summarizes it in an internal sequence embedding

$$s(e_{1:T,l}) = f_{\text{emb}}(e_{1:T,l}) \tag{14}$$

of dimension n_s. The internal sequence embedder is parameterized as a SSM (cf. Appendix D.1.1) with L_{emb} layers.

Conditioned on this sequence embedding the **latent proposal mechanism** estimates a distribution over controller latent codes z_t and samples it to produce a n_z dimensional controller latent code proposal $\tilde{z}_t$ at every timestep t. The distribution is set to be a normal

$$\tilde{z}_t \sim \mathcal{N}(\mu_t, \Sigma_t), \tag{15}$$

where Σ_t is chosen to be diagonal for computational efficiency. The parameters for mean and variance are produced by the **controller encoder**

$$\mu_t, \Sigma_t = f_{\text{enc}}\left(e_{t,l}, h_{t-1}, s\left(e_{1:T,l}\right)\right). \tag{16}$$

Crucially, if this was the final parameterization of the approximate posterior $p(z_t|e_{1:T,l})$ it would not provide a handle on the factorization of the subgoals the agent composed in time when generating its behaviour. As a first step to obtain such a factorization, the metacontroller implements a **switching unit** producing the temporal integration rate

$$\beta_t = f_{\text{switch}}(e_{t,l}, h_{t-1}, z_{t-1}) \in [0, 1]. \tag{17}$$

This integration rate is passed to the **temporal integration unit** which uses it to combine the latent code proposals $\tilde{z}_t$ sparsely in time. In particular, given β_t, $\hat{z}_t$, and z_{t-1}, the updated latent code is given by the convex combination

$$z_t = \beta_t \odot \tilde{z}_t + (1 - \beta_t) \odot z_{t-1}. \tag{18}$$

Observe, that since the $\tilde{z}_t$ are stochastically generated so is z_t. Moreover, the β_t which only rely on causal information and hence can be generated at test time provide a direct handle on the subgoals. When $\beta_t \approx 1$ a new subgoal $\tilde{z}_t$ takes over while $\beta_t \approx 0$ indicates that the previous subgoal z_{t-1} remains a valid explanation for the intent of the agent. This latent controller code z_t is then sent through the **controller decoder**. The controller decoder is a hypernetwork emitting the *internal controller*

$$U_t = f_{\text{hyp}}(z_t). \tag{19}$$

As detailed above this linear controller is applied to the residual stream to control the backbone thereby impacting the predicted data log-likelihood computed at the output of the sequence model. Crucially, the described mechanism allows the meta controller to act on extended timescales by maintaining the latent code z_k computed at timestep k for some n timesteps (by setting $\beta_{k+1:k+n-1} = 0$). Thereby, since the computation of the hypernetwork is deterministic, the same instantaneous controller U_k can be applied for n timesteps and corresponds to a temporally abstract action.

D.3 Internal RL policy architecture

Since the residual activation e_t for a single layer does not necessarily contain all information about the raw input history, we use a recurrent policy. A simple 1-layer SSM as described in section D.1.1 is used. See Table A13 and A14 for more details on the architecture.

E Additional discussions

E.1 Graphical model and ELBO derivation

Here, we present the graphical model used to derive our unsupervised objective. We denote by e_t the residual stream activation at time t, a_t the action, z_t the abstract action of which a_t is part, and β_t the random variable indicating a change in the abstract action, i.e., $z_{t-1} \neq z_t$ if $\beta_t = 1$. The assumed generative model is as follows:

$$\begin{aligned} &p(\beta_{1:T}, z_{1:T}, a_{1:T} \mid e_{1:T}) \\ =&\prod_t p(\beta_t \mid e_{1:t}) p(z_t \mid z_{t-1}, \beta_t) p(a_t \mid z_t, e_{1:t}) \end{aligned}$$

where $p(z_t \mid z_{t-1}, \beta_t) = \mathbb{1}_{z_t = z_{t-1}}$ if $\beta_t = 0$ else $\mathcal{N}(z_t \mid 0, I)$.

We want to optimize the likelihood of observing the sequence of actions by maximizing the following evidence lower bound (ELBO):

$$\begin{aligned} &\log p(a_{1:T} \mid e_{1:T}) \\ \geq &\int_{\beta,z} q(\beta_{1:T}, z_{1:T} \mid e_{1:T}, a_{1:T}) \frac{p(\beta_{1:T}, z_{1:T}, a_{1:T} \mid e_{1:T})}{q(\beta_{1:T}, z_{1:T} \mid e_{1:T}, a_{1:T})} \end{aligned}$$

where q is the variational distribution. This lower bound holds for any choice of q. Following the graphical model, q can be factorized as follows:

$$\begin{aligned} &q(\beta_{1:T}, z_{1:T} \mid e_{1:T}, a_{1:T}) \\ =&\prod_t q(\beta_t \mid e_{1:t}, a_{1:T}) q(z_t \mid z_{t-1}, \beta_t, a_{1:T}) \end{aligned}$$

where $q(z_t \mid z_{t-1}, \beta_t, a_{1:T}) = \mathbb{1}_{z_t = z_{t-1}}$ if $\beta_t = 0$ else $\mathcal{N}(z_t \mid \mu_t(a_{1:T}), \Sigma_t(a_{1:T}))$ where Σ is diagonal.

The ELBO can then be written as

$$\begin{aligned} \text{ELBO} = &\sum_t \log p_\phi(a_t \mid z_t, e_{1:t}) \\ &+ D_{\text{KL}}(q(\beta_t \mid e_{1:t}, a_{1:T}) || p(\beta_t \mid e_{1:t})) \\ &+ D_{\text{KL}}(q(z_t \mid z_{t-1}, \beta_t, a_{1:T}) || p(z_t \mid z_{t-1}, \beta_t)). \end{aligned}$$

It can be shown that the last term can be further decomposed as

$$\begin{aligned}&D_{\mathrm{KL}}(q(z_t \mid z_{t-1}, \beta_t, a_{1:T}) || p(z_t \mid z_{t-1}, \beta_t)) \\ =&\begin{cases} 0 & \text{if } \beta_t = 0 \\ D_{\mathrm{KL}}(\mathcal{N}(z_t \mid \mu_t(a_{1:T}), \Sigma_t(a_{1:T})) || \mathcal{N}(0, I)) & \text{if } \beta_t = 1. \end{cases}\end{aligned}$$

Continuous relaxation. In order to improve stability during training, we make a continuous relaxation of the latent variable β sampled. In principle, this can be done with the Gumbel-Sigmoid trick, but in our experiments we simply used the probability as the latent variable.

We modify the prior and variational distribution on z to be the continuous relaxation, i.e.,

$$\begin{aligned}&p(z_t \mid z_{t-1}, \beta_t) = \mathcal{N}(z_t \mid (1-\beta_t) z_{t-1}, \beta_t^2 I) \\ &q(z_t \mid z_{t-1}, \beta_t, a_{1:T}) \\ &= \mathcal{N}(z_t \mid \beta_t \mu_t(a_{1:T}) + (1-\beta_t) z_{t-1}, \beta_t^2 \Sigma_t(a_{1:T})).\end{aligned}$$

This recovers the previous behavior when β_t equals 0 or 1.

In the continuous case, it can be shown that the KL divergence is

$$\begin{aligned}&D_{\mathrm{KL}}(q(z_t \mid z_{t-1}, \beta_t, a_{1:T}) || p(z_t \mid z_{t-1}, \beta_t)) \\ =&D_{\mathrm{KL}}(\mathcal{N}(\mu_t(a_{1:T}), \Sigma_t(a_{1:T})) || \mathcal{N}((0, I)).\end{aligned}$$

Further assumptions. In our experiments, we further modify the variational distribution on β such that $q(\beta_t \mid e_{1:t}, a_{1:T}) \approx q(\beta_t \mid e_{1:t})$, i.e., we drop the conditioning on the future. This is done such that during internal RL, the switching signal can be emitted causally, and eliminates the prior matching term for the switching module. This assumption was made in our experiments since we assumed the residual activation to be highly informative of when switches should occur, in the environments considered. In general however, we can relax this assumption by keeping the future conditioning, but distilling the switches to an unconditioned module.

E.2 Internal RL vs RL with reparametrization trick

As explained in Section C.5.1, internal RL learns a policy over the discovered abstract action space of z by treating the rest of the architecture as part of the environment, and applying reinforcement learning directly to z, with temporal abstraction. However, there are other ways to use the discovered abstract actions than the proposed internal RL. One perhaps more straightforward way to use the metacontroller, is to treat this policy as a noise-injecting submodule of the overall architecture which is still trained by reinforcement learning in raw action space, by backpropagating through the base autoregressive model, to the policy using e.g. the reparametrization trick. In this section, we analytically contrast these 2 options, discuss their respective advantages, and motivate why we believe the internal RL is interesting in general.

To simplify the analyses, we make a few assumptions:

- We remain in the outcome-supervision setting: a single reward r_T is provided at the last time step T.
- The switching happens M times, at $(t_m)_{1 \le m \le M}$.
- The abstract action policy has a fixed variance, i.e., it outputs $z_t = \mu(s_t) + \epsilon_t$ where s_t is the history of observations up to t, $\epsilon_t \sim \mathcal{N}(0, 1)$.

We now contrast the policy gradient update of the abstract action policy, between the 2 options discussed above.

Raw action space RL. Performing RL in raw action space, treating the abstract action policy as a model layer, would result in the following expected policy gradient update:

$$
\begin{aligned}
&\mathbb{E}\left[r_T \sum_{t=1}^{T} \nabla_\phi \log \pi(a_t \mid s_t, z_t)\right] \\
&= \mathbb{E}\left[r_T \sum_{m=1}^{M} \sum_{t=t_m}^{t_{m+1}-1} \nabla_\phi \log \pi(a_t \mid s_t, z_{t_m})\right] \\
&= \mathbb{E}\left[r_T \sum_{m=1}^{M} \Big[\sum_{t=t_m}^{t_{m+1}-1} \nabla_{z_{t_m}} \log \pi(a_t \mid s_t, z_{t_m})\Big] \nabla_\phi(\mu(s_{t_m} + \epsilon_{t_m}))\right] \\
&= \mathbb{E}\left[r_T \sum_{m=1}^{M} \Big[\sum_{t=t_m}^{t_{m+1}-1} \nabla_{z_{t_m}} \log \pi(a_t \mid s_t, z_{t_m})\Big] \nabla_\phi \mu(s_{t_m})\right].
\end{aligned}
$$

Internal RL. In contrast, internal RL (i.e., RL directly in z-space) results in the following policy gradient update:

$$
\begin{aligned}
&\mathbb{E}[r_T \sum_{m=1}^{M} \nabla_\phi \log P(z_{t_m} \mid s_{t_m})] \\
&= \mathbb{E}[r_T \sum_{m=1}^{M} \nabla_\phi \frac{-1}{2}(z_{t_m} - \mu(s_{t_m}))^2] \\
&= \mathbb{E}[r_T \sum_{m=1}^{M} \epsilon_{t_m} \nabla_\phi \mu(s_{t_m})].
\end{aligned}
$$

Note that since the forward pass is the same for both methods, the distribution over trajectory and rewards are identical. Let us then compare the variance of these 2 estimators. For simplicity, we now further assume $M = 1$. This means a single z is drawn at the beginning of the sequence. The law of total variance gives

$$
\begin{aligned}
&\mathbb{V}\big[r_T \big[\sum_t \nabla_z \log \pi(a_t \mid s_t, z_0)\big] \nabla_\phi \mu(s_0)\big] \\
&= \mathbb{V}\big(\mathbb{E}\big[r_T \sum_t \nabla_z \log \pi(a_t \mid s_t, z_0) \mid z_0\big] \nabla_\phi \mu(s_0)\big) \\
&\quad + \mathbb{E}\big(\mathbb{V}\big[r_T \sum_t \nabla_z \log \pi(a_t \mid s_t, z_0) \mid z_0\big] \nabla_\phi \mu(s_0)\big) \\
&= \mathbb{V}\big(\mathbb{E}\big[\mathrm{PG}_{\mathrm{raw}}(z_0)\big] \nabla_\phi \mu(s_0)\big) + \mathbb{E}\big(\mathbb{V}\big[\mathrm{PG}_{\mathrm{raw}}(z_0)\big] \nabla_\phi \mu(s_0)\big)
\end{aligned}
$$

where $\mathrm{PG}_{\mathrm{raw}}(z) = r_T \sum_t \nabla_z \log \pi(a_t \mid s_t, z)$ is the raw action space policy gradient Monte Carlo estimator w.r.t. "parameter" z.

Similarly,

$$
\begin{aligned}
&\mathbb{V}\big[r_T \epsilon_0 \nabla_\phi \mu(s_0)\big] \\
&= \mathbb{V}\big(\mathbb{E}\big[r_T \mid \epsilon_0\big] \epsilon_0 \nabla_\phi \mu(s_0)\big) + \mathbb{E}\big(\mathbb{V}\big[r_T \mid \epsilon_0\big] \epsilon_0 \nabla_\phi \mu(s_0)\big) \\
&= \mathbb{V}\big(\mathbb{E}\big[\mathrm{PG}_{\mathrm{z}}(z_0)\big] \nabla_\phi \mu(s_0)\big) + \mathbb{E}\big(\mathbb{V}\big[\mathrm{PG}_{\mathrm{z}}(z_0)\big] \nabla_\phi \mu(s_0)\big)
\end{aligned}
$$

where $\mathrm{PG}_{\mathrm{z}}(z) = r_T \epsilon_0$ is the policy gradient Monte Carlo estimator of a bandit problem.

We see that the 2 expressions differ only in $\mathrm{PG}(z)$. The tradeoffs are evident:

- The expectation of $\mathrm{PG}_{\mathrm{raw}}$ is more structured than PG_{z}. In particular, its variance w.r.t. epsilon could even be 0 in the first, whereas it scales with the dimension of epsilon in the second.
- However, the variance of $\mathrm{PG}_{\mathrm{raw}}$ scales with the number of timestep and with the raw action space dimension, since noise is accumulated at every timestep. On the other hand, PG_{z}

does not scale with anything (it is the variance of the return, i.e., $O(1)$). Therefore, if the abstract action discovery was successful such that a compact space of z was identified, with long-horizon abstract actions, the policy gradient estimator's variance and corresponding credit assignment can be dramatically improved, especially for very long horizon tasks.